PHYSICS IN THE NEUTRON STAR CRUST AND GLITCH PHENOMENA

by

Onur Akbal

Submitted to the Graduate School of Engineering and Natural Sciences
in partial fulfillment of
the requirements for the degree of
Doctor of Philosophy

Sabancı University
Summer 2016

PHYSICS IN NEUTRON STAR CRUST AND GLITCH PHENOMENA

APPROVED BY

Prof. Dr. Mehmet Ali Alpar
(Thesis Supervisor) .....

Assoc. Prof. Dr. Ünal Ertan .....

Prof. Dr. Kazım. Yavuz Ekşi .....

Prof. Dr. Canan Atılgan .....

Prof. Dr. Mustafa Türker Özkan .....

DATE OF APPROVAL 09. 08. 2016

PHYSICS IN THE NEUTRON STAR CRUST AND GLITCH PHENOMENA

Onur Akbal

Physics, Doctor of Philosophy Thesis, 2016

Thesis Supervisor: Prof. Dr. Mehmet Ali Alpar

Abstract

Glitches are sudden changes in rotation frequency and spin-down rate, observed from pulsars of all ages. Standard glitches are characterized by a positive step in angular velocity ($\Delta\Omega > 0$) and a negative step in the spin-down rate ($\Delta\dot{\Omega} < 0$) of the pulsar.

There are no glitch-associated changes in the electromagnetic signature of rotation-powered pulsars most cases. For the first time, in the last glitch of PSR J1119-6127, there is clear evidence for changing emission properties coincident with the glitch. This glitch is also unusual in its signature. Further, the absolute value of the spin-down rate actually decreases in the long term. This is in contrast to usual glitch behaviour. In the first Chapter the vortex creep model is extended in order to take into account these peculiarities. It is proposed that a starquake with crustal plate movement towards the rotational poles of the star induces inward vortex motion which causes the unusual glitch signature. The component of the magnetic field perpendicular to the rotation axis will decrease, giving rise to a permanent change in the pulsar external torque.

The vortex creep model explains the postglitch behaviour of Vela pulsar well, while it has the difficulties to estimate the interglitch time intervals. In the second Chapter it is hypothesized that for each Vela glitch there might be a persistent shift, which will not relax back, in the post-glitch "triangle" fashion of $\Delta\dot{\Omega}$. This step would not be distinguished observationally at the time of the glitch. The modified expression for the time between glitches by using this consideration is applied for 14 Vela glitches by minimizing rms deviations between the model and observed glitch times. The estimates are in better agreement with the observed values with the persistent shift of $\Delta\dot{\Omega}_p/\dot{\Omega} = 1.6 \times 10^{-3}$ for all Vela glitches. Different $\Delta\dot{\Omega}_p$ values for each Vela glitch are also calculated by inserting the observed interglitch times in the modified expression.

Glitches are triggered by an initial crust breaking event. The size of the crust breaking is determined by the critical strain angle, θ_{cr}. The broken crust plate size in turn determines the number of vortices involved in the unpinning avalanche that effects the size of

the amplified glitch. The event of minimum glitch size of the Crab pulsar observed by Espinoza et al. (2014) is investigated in the third Chapter. Modelling the "pure" crustquake as a trigger mechanism with some breaking geometries, some physical quantities in neutron star crust, like the size of the broken plate, the critical strain angle at which fracture occurs, and the number of triggered vortices involved in larger glitches are estimated.

In the final Chapter the critical strain angle in the Coulomb crystal in the neutron star crust is estimated on the assumption that this dimensionless number is of the order of the ratio of the Coulomb potential energy to the kinetic energy of the relativistic electrons, $\theta_{cr} \sim |E_C|/E_K$. This estimate scales with the fine structure constant, the charge Z, and microscopic length scales. The scaling also depends on the dimensionality according to the shapes of the nuclear clusters in various "pasta" geometries (i.e. spherical, rod, slab) in the inner crust. It is found that $\theta_{cr} \sim 10^{-1}$ in the outer crust, in agreement with the numerical results of Horowitz & Kadau (2009), while it reduces to $10^{-2} - 10^{-3}$ in the inner crust where the lower dimensional rod and slab configurations prevail. Screening which is very weak does not change the results appreciably.

NÖTRON YILDIZI KABUĞUNUN FİZİĞİ VE SIÇRAMA OLGUSU

Onur Akbal

Fizik, Doktora Tezi, 2016

Tez Danışmanı: Prof. Dr. Mehmet Ali Alpar

Özet

Pulsar sıçramaları, yıldızın açısal dönme hızında ani bir artış olarak gözlenir. Bu artış sıçrama öncesi periyoda göre $\Delta\Omega/\Omega = 10^{-9} - 10^{-6}$'lık kesirsel bir azalmaya karşılık gelir. Dönme hızındaki bu sıçramaya ek olarak yıldızın yavaşlama oranının mutlak değeri de sıçrama öncesindeki değerine göre bir artış gösterir. Bu artış kesirsel olarak $\Delta\dot{\Omega}/\dot{\Omega} = 10^{-4} - 10^{-1}$ mertebesindedir.

Tezin ilk bölümünde yüksek manyetik alanlı bir pulsar olan PSR J1119-6127 kaynağının standart sıçrama parametrelerine (yıldızın dönme oranındaki artışı, yavaşlama oranının büyüklüğündeki artış ve sıçrama sırasında pulsarın emisyon özelliklerinde bir farklılık gözlenmemesi gibi) aykırı özellikler içeren 2007 yılı sıçramasını vorteks sızma modeli çerçevesinde incelendi. Gözlemsel anlamda bu aykırı özellikler iki maddede toplanabilir: (i) Yıldız, sıçrama sonrasında sıçrama öncesine göre daha düşük bir yavaşlama oranı ile yavaşlamaktadır, (ii) bu sıçrama ile birlikte, yıldızın dış tork değişimine işaret eden emisyon özelliklerinde geçici farklılıklar ortaya çıkmıştır. Vorteks sızma modeli bu ki acayip davranışı hesaba katılacak şekilde geliştirildi. Sıçrama ile birlikte dış torkta da bir değişimin meydana gelmesi ve yavaşlama oranında da kalıcı bir değişiklik oluşması yıldızın kabuğunda meydana gelen olası bir deprem ile açıklanmaya çalışıldı. Buna göre deprem sırasında kabuk parçası yıldızın manyetik kutbuna doğru hareket eder kabuğa bağlı manyetik alan çizgilerinin elastiki yapıları yıldız emisyon özelliğinde belli bir süre değişiklik meydana getirir.

Vorteks sızma modeli, Vela pulsarının sızma sonrası davranışlarını başarılı bir şekilde açıklayabilse de, iki sıçrama arasındaki zaman tahmini konusunda zorlukları vardır. Bu tezin ikinci bölümünde Vela pulsarının sıçramaları ele alınarak sızma modelinin öngördüğü sıçramalar arası geçen zaman ifadesinde iyileştirmeler yapılmış ve gözlemler ile teorik sonucun uyumluluğu araştırılmıştır. Gözlemler çoğunlukla Vela kaynağının iki sıçrama arasındaki zamanının, modelin tahmin ettiğinden daha kısa olduğunu gösteriyor. Modele değişiklik getirirken önerilen senaryo şudur: Vela pulsarı da Yengeç pulsarı gibi deprem tarafından tetiklenen bir sıçrama meydana getiriyor ise yıldızın yavaşlama oranında kalıcı

bir azalma olacaktır. Sızma teorisine göre bu kalıcı azalma depremin tetiklediği yeni vortex boşalma bölgelerinden kaynaklanmaktadır. Bu yeni bölgeler sıçramadan önce vorteks sızmasına katkıda bulunuyorken, olay sonrası spin yavaşlama oranına katkı sağlamayacaktır. Vela pulsarında yavaşlama oranındaki bu kalıcı değişim sıçrama büyüklüğü içinde gözlemlerden kaçmış olabilir. Buna göre bir sonraki sıçrama zamanının doğrusal olarak daha kısa bir sürede olması gerekmektedir. Analizler sonucu Vela sıçramaları için bulduğumuz, gözlem değerlerine en çok yaklaştıran yıldızın yavaşlama oranındaki kalıcı değişikliğin kesirsel değeri $\Delta\dot{\Omega}_p/\dot{\Omega} = 1.6 \times 10^{-3}$'tür.

Pulsar sıçramaları yıldız depremleri ile tetiklenen olaylardır. Yıldız kabuğunun kırılması, kritik kırılma açısı ile belirlenir. Bu da sıçrama ile etkilenen daha büyük sıçramalara yol açan toplam vorteks sayısı ile ilişkilidir. Üçüncü bölümde Crab pulsarında gözlemlenen en üçük sıçrama olayı yıldız depremi modeli ile incelenmiştir.

Tezin son bölümünde yıldız kabuğunun farklı tabakalarında deprem koşullarının oluşumu için gerekli kritik gerilme açısının eğeri elde edilmiştir. Nükleer pasta yapıları da ele alınarak bir Wigner-Seitz hücresi içersindeki toplam elektriksel Coulomb potensiyel enerjisinin, çekirdek etrafındaki elektronların hareketinden meydana gelen toplam kinetik enerji oranı bulundu. Bu boyutsuz değerin kritik gerilme açısı ile doğrudan ilişkili olma yorumundan yola çıkarak kabuğun farklı katmanlarınlaki $/theta_{kr}$ değerleri elde edildi. Buna göre yıldızın kabuğunda meydana gelecek bir deprem iç tabakalarda daha olası iken, dış tabakaya doğru zorlaşır.

ACKNOWLEDGEMENTS

I deeply appreciate my supervisor, M. Ali Alpar, who accepted me as his student and guided me along this thesis. His door has always been open for any question, discussion. He always inspires me to simplify the complex problems.

I would also like to thank my friends and colleagues, Sinem Şaşmaz Muş, Erbil Gügercinoğlu, Efe İlker, İskender Yalçınkaya, Tolga Çağlar and Onur Benli, for the scientific discussions, enjoyable lunches and drinking.

I also want to thank my father, İrfan. He always supported for my education and encouraged me to finish my PhD.

Finally I owe very special thanks to my wife, Merve, for her all love and understanding. I dedicate this thesis to her.

Contents

ABSTRACT iv

ÖZET vi

ACKNOWLEDGEMENTS viii

1 INTRODUCTION 1
1.1 The Structure and Formation of Isolated Neutron Stars 2
1.1.1 Layered Structure of the Crust 3
1.1.2 The Outer Core 4
1.1.3 Superfluidity 4
1.2 Spinning down of Pulsars and The Braking Index 6
1.3 Pulsar Timing and the Irregularities: Glitches and Timing Noise 8
1.3.1 Timing Noise 8
1.3.2 Glitches 10

2 PECULIAR GLITCH OF PSR J1119-6127 AND EXTENSION OF THE VORTEX CREEP MODEL 13
2.1 Introduction 14
2.2 The Peculiar Glitch of PSR J1119-6127 15
2.3 Overview of the Vortex Creep Model 16
2.4 Extension of the Vortex Creep Model 19
2.5 Model Fits 22
2.6 Discussion and Conclusions 26

3 INTERGLITCH TIME INTERVALS OF THE VELA PULSAR 35
3.1 Introduction 36
3.2 Model Fitting 40
3.3 The Modified Interglitch Times of the Vela Pulsar 41
3.4 The Braking Index of the Vela Pulsar 45
3.5 Conclusions 46

4 MINIMUM GLITCH SIZE OF THE CRAB PULSAR AND THE CRUSTQUAKE AS A TRIGGER MECHANISM 48
4.1 Introduction . . . 49
4.2 Geometry of the Crustquake and Some Estimates . . . 50
4.2.1 Size of the Broken Plate(s) . . . 52
4.2.2 The Critical Strain Angle . . . 53
4.2.3 Number of Vortices Involved in a Larger Glitch . . . 54
4.3 Conclusions . . . 55

5 THE CRITICAL STRAIN ANGLE IN THE NEUTRON STAR CRUST 57
5.1 Introduction . . . 58
5.2 The Coulomb Potential Energy and the Kinetic Energy in a Unit Cell . . . 60
5.3 Estimation of the Critical Strain Angle in the Crust . . . 61
5.3.1 The Screening Effect . . . 65
5.4 Discussion and Conclusions . . . 67

BIBLIOGRAPHY 77

List of Figures

1.1 Schematic view of a neutron star structure, in the ground state, throughout the density. Figure credit: The review paper of Chamel & Haensel (2008) 3

1.2 The typical interior structure of a neutron star and types of superfluids along the density. Figure credit:http://slideplayer.com/slide/4522702/ . . . 5

1.3 Schematic picture of the rotating magnetic dipole model. As illustrated here, the rotational axis is misaligned with the magnetic field axis which is almost aligned with the radiation beam. Figure credit: The Phd thesis of Danai Antonopoulou 6

1.4 The glitch candidates of the Crab pulsar along the times. Horizontal lines show the limit of glitch detection. Figure Credit: Paper by Espinoza et al. (2014) 9

1.5 Schematic illustration of some typical glitch recoveries. Figure Credit: The Phd thesis of Danai Antonopoulou 11

2.1 Top panel: Fit to the post-glitch spin-down rate data with the model of Equation (2.15), with $\Delta = 60$ days and b = 1.0×10^{-13} rad s^{-2}. Middle panel: Zoomed version of top panel with model components representing contribution of exponential relaxation term (purple solid line), inward moving vortices (gray dashed line) and outward moving vortices (blue dash dotted line) are shown separately. Sinusoidal component and long-term offset b are not shown in the figure for clarity. Bottom panel: Difference between data and model. 24

2.2 Starquake Model in cross section. The dotted area represents new position of crustal plates (broken ring) after the starquake. 33

3.1 The inferred model fits with the observations of the post-glitch spindown rate of the 1996, 2000, 2004, 2006, 2010 Vela glitches. In the bottom panels the discrepancy between data and model is showed. 42

3.2 The schematic view of the long term behaviour of $\Delta\dot{\Omega}/\dot{\Omega}$ 43

3.3 The spin-down rate values obtained by the local fits at the epochs t'_g (black points), t_{obs} (red points), and t_g (green points) between the years of 1969 and 2013. The best straight line fits is also showed. 46

4.1 Geometries of crust breaking in spindown of the neutron star: (a) a crustal cubic plate, (b) a cylindrical plate moving towards the rotational axis, and (c) a crustal ring, including many plates, moving inward in cylindrical symmetry 51

5.1 Critical strain angle values vs density in the outer crust where the nuclei are spherical Plus signs denote the values of θ_{cr} calculated with the bare Coulomb interaction, bold dots are the values of θ_{cr} calculated with the screened Coulomb interaction. The values of proton number, Z, and the Wigner-Seitz cell size, r_c, are taken from Chamel and Haensel. Square dots at $n_b = 0.006$ fm^{-3} indicate the numerical results of Horowitz & Kadau (2009) for different crystalline structures and strain orientations (see their Figure 1). 62

5.2 Critical strain angle values vs density in the inner crust comprising the 'pasta' layers. Plus signs denote the values of θ_{cr} calculated with the bare Coulomb interaction, bold dots are the values of θ_{cr} calculated with the screened Coulomb interaction. The values of nucleus size, R, and the Wigner-Seitz cell size, r_c, are taken from Maruyama et al. (2005). 63

5.3 Critical strain angle values vs density in the inner crust comprising the 'pasta' layers. Plus signs denote the values of θ_{cr} calculated with the bare Coulomb interaction, bold dots are the values of θ_{cr} calculated with the screened Coulomb interaction. The values of nucleus size, R, and the Wigner-Seitz cell size, r_c, are taken from Iida, Watanabe & Sato (2001). . 64

List of Tables

2.1 Parameters of the best fits to the postglitch frequency derivative data following the 2007 glitch of PSR J1119-6127, with $\Delta = 60$ days, and $b = 1.0 \times 10^{-13} rad\ s^{-2}$ (first column) and $b = 0$ (second column) 25

2.2 Inferred Parameters with $b = 1.0 \times 10^{-13} rad\ s^{-2}$. 25

3.1 The inferred and observed parameters for the long term response of the Vela glitches. The entries for the first eight glitches and the ninth glitch are taken from Alpar et al. (1993) and Chau & Cheng (1993) respectively. Errors for the last five parameters are also given in parenthesis. 41

3.2 Modified interglitch time estimates with the observation times and fit parameters of Vela glitches with the persistent shift in spindown rate of $\Delta\dot{\Omega}_p/\dot{\Omega} = 1.6 \times 10^{-3}$ rad s^{-2} 44

3.3 The persistent steps in spindown rate and associated fit parameters of Vela glitches, needed to give $t'_g = t_{obs}$ 45

Chapter 1

INTRODUCTION

Neutron star is a celestial body which is one of the expected outcomes of stellar evolution, with the white dwarfs and black holes, after supernova explosions. A star without the fuel cannot manufacture its own energy to maintain the pressure against its own gravity at the end of its life, leading a sort of subsequent collapse. In the stars with low mass (like our sun), the pressure of degenerate electrons can balance gravity, leaving behind a "white dwarf", while the collapse proceeds for heavier stars. As the matter in the central region becomes so intense, the atomic nuclei dissolves into a mixture of electrons protons and mostly degenerate neutrons which can provide an effective pressure against gravity, leave another type of remnant, neutron star. It is also thought that if the pressure in the neutron star is not sufficient, the collapse then cannot be stopped and the "black hole" is created.

Pulsars (Pulsating Radio Stars) rotate extremely fast. They are observed with the rotational periods varying between 1.4 ms $< P < 12$ sec [1]. Such high velocities in neutron stars are due to angular momentum conservation as a result of the collapse of the progenitor. Their periods also increase in time with a very slow rate, typically $\dot{P} \sim 10^{-15}$ Hz s^{-1}, due to the loss of rotational energy.

In 1967 Jocelyn Bell Burnell, who discovered PSR B1919+21 (Hewish et al., 1968), firstly observationally confirmed the presence of neutron stars. Gold (1968) firstly proposed the idea that there must be a link between the pulsars and neutron stars and modelled a rotating magnetised neutron star. This was also confirmed by the discoveries of the pulsed emission from the Vela pulsar (Large, Vaughan & Mills, 1968) and the Crab pulsar (Staelin & Reifenstein, 1968) in supernova remnants.

1.1 The Structure and Formation of Isolated Neutron Stars

Neutron stars, the densest and very strongly magnetized bodies known, are convenient laboratories to research the nature in such extraordinary conditions. They have a mass above that of the Sun, squeezed into a radius of approximately 10 km so that the density inside is greater than the nuclear saturation density ($\rho_0 = 2.8 \times 10^{14}$ g cm^{-3}) which cannot be examined in terrestrial materials. The description of the equation of state still remains unknown at such high densities, but there are some possible suggestions. Oppenheimer & Volkoff (1939) firstly tried to calculate the equation of state and predicted that the neutron stars have a maximum mass of 0.7 $M_\odot$, assuming that a star is only formed by noninterracting neutrons. The recent works by Demorest et al. (2010); Antoniadis et al. (2013) though observed the maximum mass of the neutron star around $(2-3)$ $M_\odot$.

[1] The Australia Telescope National Facility Pulsar Catalogue (Manchester et al., 2005)

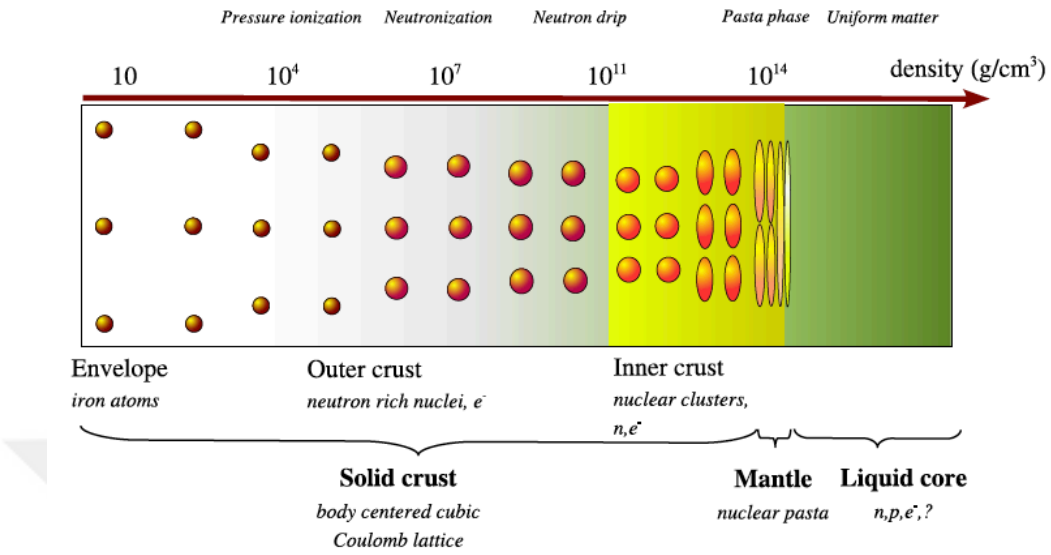

Figure 1.1: Schematic view of a neutron star structure, in the ground state, throughout the density. Figure credit: The review paper of Chamel & Haensel (2008)

1.1.1 Layered Structure of the Crust

Though the temperature inside the neutron stars is $\gtrsim 10^7$ K, they are indeed thought to be as cold objects due to the fact that the Fermi energy is larger than the thermal energy in such high densities. It is assumed that the matter inside is already in thermodynamical equilibrium at zero temperature and in its ground state with the lowest energy. Figure 1.2 visualizes the layered structure of the crust in the ground state. The neutron drip density, $\rho_{drip} = 4 \times 10^{11}$ g cm^{-3}, separates the crust into two regions: the outer crust and the inner crust.

The outer region of crust, constituted by electrons and nuclei, is formed of a body centred cubic lattice (bcc) with mostly ^{56}Fe atom (Chamel & Haensel, 2008). The atoms are already ionized at the surface where $\rho \sim 10^4$ g cm^{-3}. Due to electron captures, the nuclei turns into neutron-rich composition at densities above $10^6 - 10^7$ g cm^{-3}. The degenerate electrons are uniformly distributed and relativistic everywhere but in the most outer layer with a few meters thick. Screening effect in the Coulomb interactions can be negligible as the Thomas-Fermi screening length is larger than the lattice spacing Pethick & Ravenhall (1995).

The inner crust, extending from the neutron drip density to $\rho \sim 3 \times 10^{14}$ g cm^{-3}, is composed of the neutron-rich nuclei together with the electron gas and free neutrons, containing a BCS superfluid by pinning as a result of neutron-neutron interactions[2]. The ratio of free neutrons increases towards the bottom layers and finally the nuclei entirely dissolve. At the deepest region ($\rho \sim 3 \times 10^{14}$ g cm^{-3}), there is a series of phase transitions to the core with nuclei that are arranged in rod and slab, instead of spherical forms, the so called "pasta" phases Ravenhall, Pethick & Wilson (1983); Hashimoto, Seki & Yamada (1984).

1.1.2 The Outer Core

The region of the outer core where the density reaches to $\rho \sim 5 \times 10^{14}$ g cm^{-3} is expected to be composed of a few percentage of protons, electrons, muons, and mostly neutrons. While the electrons and muons are thought to be as an ideal fermionic gas, the neutrons and protons are in the formation of superfluid state as a result of a strong interaction. The protons in this region are expected to be in a formation of a type II superconductor with the magnetic flux concentrated in flux-tubes Baym et al. (1969). There is also a strong interaction between the vortices of superfluid neutron and flux tubes, leading to pinning in the core.

1.1.3 Superfluidity

The explanation of superconductivity for the terrestrial materials with low resistivity was firstly given by Bardeen, Cooper & Schrieffer (1957). According to this BCS theory, it is energetically favourable for the fermions in a system (for instance electrons in metals) to produce boson-like states by a condensation of cooper pairs at sufficiently low temperature. Superfluids with almost zero viscosity are neutral, while superconducting currents are charged.

Migdal (1959) firstly proposed the idea of the existence of superfluidity and superconductivity inside neutron stars with the analogy of electrons in superconductor. Nucleons in neutron star, with high density and low temperature, can also create cooper pairs as a result of attractive nuclear forces (Bohr, Mottelson & Pines, 1958; Cooper, Mills & Sessler, 1959). Superfluid inside neutron star is classified as three types: neutron superfluid with the form of $^1S_0$ in the inner crust, neutron superfluid (with $^3P_2$ pairing) and $^1S_0$ superconducting proton inside the core (Figure 1.3). The outermost crust lacks of superfluid as the nucleon density is not high enough there. As density increases to neu-

[2] see the following section for more details about the superfluidity in the inner crust

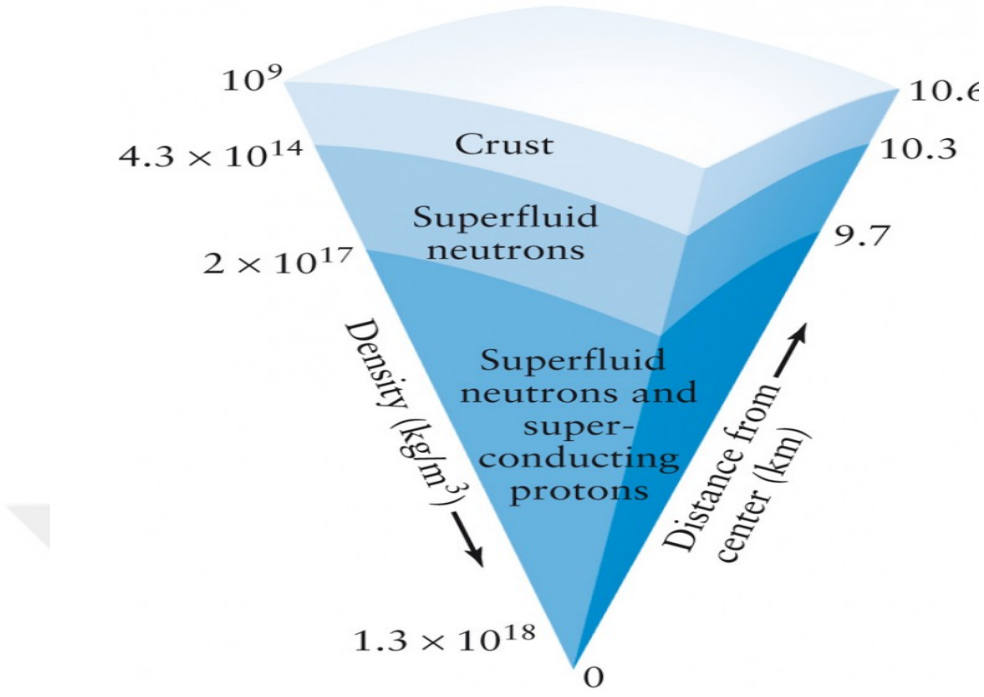

Figure 1.2: The typical interior structure of a neutron star and types of superfluids along the density. Figure credit:http://slideplayer.com/slide/4522702/

tron drip density more and more free neutrons produce continuum states of fermi sea and configure cooper pairs by the long range attractive interaction. In these densities protons cannot form superfluid since they still remain locked inside nucleus. In the core region the density is high enough so that all neutrons and protons are free of bound states and can form in superfluid and superconductor respectively. The prediction of the existence of superfluidity has been recently verified by monitoring the cooling of the young NS in the supernova remnant Cassiopeia A (Shternin et al., 2011; Page et al., 2011).

It is energetically favourable for the superfluid inside the rapidly rotating crust (container) to follow the rotation. This is obtained by the weak interactions between the normal component and vortices carrying the quantized circulation $\kappa = h/2m_n$, where h is the Planck constant and $2m_n$ is the mass of a neutron pair. The rotational rate of superfluid component is found by the vortex density, so there is a connection between vortex motion inside neutron star and the superfluid velocity. It is well established from the experiments of Helium II that superfluid can rotate by the quantized vortices carrying the circulation. The details about the superfluid dynamics and its relation with the crustal lattice are given in the next chapters.

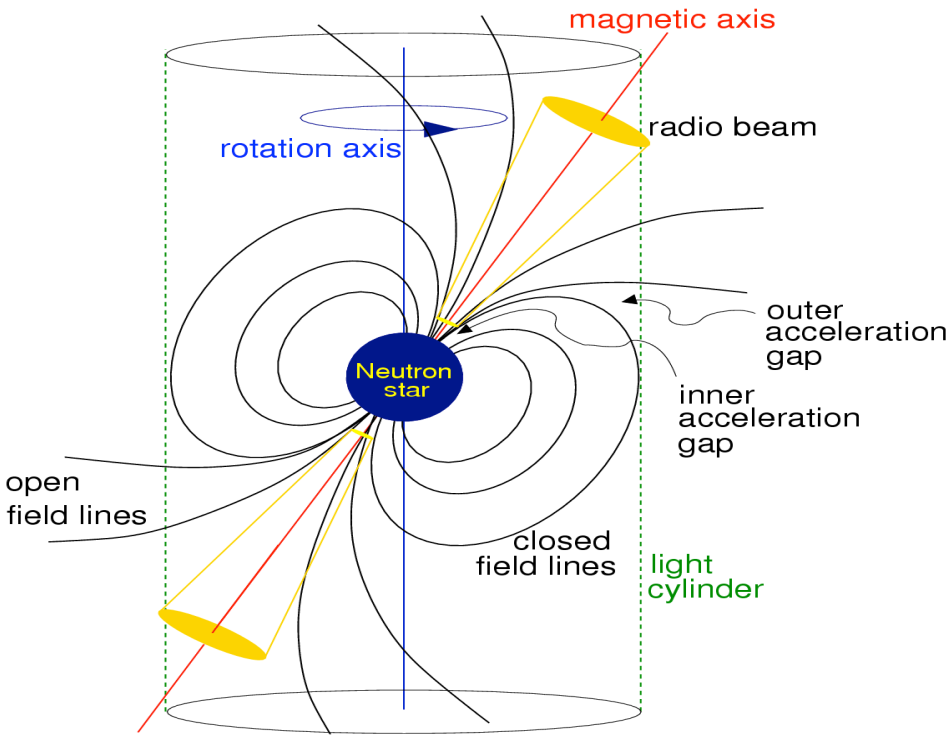

Figure 1.3: Schematic picture of the rotating magnetic dipole model. As illustrated here, the rotational axis is misaligned with the magnetic field axis which is almost aligned with the radiation beam. Figure credit: The Phd thesis of Danai Antonopoulou

1.2 Spinning down of Pulsars and The Braking Index

The rotating magnetic dipole model, which is not a full picture though, attempts to explain the spinning down and pulsation of neutron star. This model (Figure 1.4) involves the magnetic field axis which is aligned with the radio emission beam, but misaligned with respect to the rotational axis (Ruderman & Sutherland, 1975). The accelerated particles on the surface, induced by the magnetic field and rotation with the pair creation process, form a rigid magnetosphere that rotates with the pulsar (Goldreich & Julian, 1969). These charged particles in the magnetosphere produce a narrow beam emission, also aligned with the magnetic axis. This is observed as a radiation pulse with a frequency which equals to the rotational frequency of pulsar (Eastlund, 1968; Ginzburg & Zaitsev, 1969).

In the model the magnitude of the magnetic moment is given by

$$|m| = \frac{B_{\perp} R^3}{2} \tag{1.1}$$

where R is the radius of neutron star and $B_\perp$ is the perpendicular component of the magnetic field with respect to the rotational axis. The nonalignment of the magnetic moment with respect to the rotational axis makes the magnetic moment changing with time. This, just as an accelerated charge, causes the rate of energy loss that is given by

$$\dot{E}_{dip} = -\frac{2}{3c^3}|\ddot{m}|^2 = -\frac{B_\perp^2 R^6 \Omega^4 sin^2\alpha}{6c^3} \tag{1.2}$$

where α is the angle rotational axis and magnetic moment. This energy comes from the rotational kinetic energy of a pulsar, giving the radio luminosity as

$$\dot{E}_{rot} = I\Omega\dot{\Omega}. \tag{1.3}$$

Here $I \sim 10^{45}$ gm cm^2 is the inertial moment of star. The pulsar spins down as a result of the torque exerted by the radiation. The magnetic braking rate is found equating these two relations:

$$\dot{\Omega} = -\frac{2B_\perp^2 R^6 \Omega^3}{3Ic^3} \tag{1.4}$$

which gives an estimate for $B_\perp$ from the observations of P and $\dot{P}$. From Equation (1.3) the spindown rate can be generally related with the angular velocity as $\dot{\Omega} = -K\Omega^n$. Here the exponent n is the braking index and K is a factor that generally depends on inertial moment and magnetic moment. On the assumption that K and n are constant during a lifetime of a pulsar, differentiation of the spindown power gives

$$n = \frac{\Omega\ddot{\Omega}}{(\dot{\Omega})^2} \tag{1.5}$$

which can be obtained by the measurement of $\ddot{\Omega}$. The spindown (characteristic) age of pulsar can also be roughly estimated by

$$\tau = \frac{-\Omega}{(n-1)\dot{\Omega}} \tag{1.6}$$

with the assumption that pulsar had a very high angular velocity in initial stage. To date all braking indices have been measured as less than 3 (see Archibald et al. (2016) for an exception), suggesting that the rotating magnetic dipole model is not sufficient to explain the pulsar long term spindown (Lyne, Pritchard & Graham-Smith, 1993; Livingstone

et al., 2007; Roy, Gupta & Lewandowski, 2012) and other alternatives must be included (Blandford & Romani, 1988; Chen & Li, 2006; Ho & Andersson, 2012; Antonopoulou et al., 2015)

The measurement of n can be possible for very few pulsars like Crab, PSR B0540-69, PSR B1509-58, PSR J1119-6127 which are young. Such a measurement can be difficult for older pulsars due to high levels of timing irregularities (i.e. timing noise, glitches) which create a sort of contamination in steady spindown.

1.3 Pulsar Timing and the Irregularities: Glitches and Timing Noise

Pulsar timing[3] is the process of the regular monitoring of the neutron star rotation over long periods. Tracking (highly precisely) the times of arrival of the radio pulses, astronomers obtain some physical information including the magnetosphere and interior of neutron stars, such as their age and magnetic field.

After extracting some astronomical effects, like the pulsar's proper motion and the Earth's orbital motion, and determining the time of arrival (TOA) of each pulse, the spin frequency is evaluated using Taylor expansion around the epoch t_0:

$$\nu(t) = \nu_0 + \dot{\nu}_0(t - t_0) + \frac{1}{2}\ddot{\nu}_0(t - t_0)^2 \tag{1.7}$$

where subindex 0 denotes the parameters at time $t = t_0$. The rotational parameters of a pulsar are found by timing residuals between observation and the above model. Pulsars in general show the rotational stability, which makes them the most precise clocks in the universe. But there are also two remarkable irregularities from this trend: (i) random and slow deviation from Equation (1.6), called "timing noise", and (ii) abrupt changes in rotational frequency and its derivative, glitches.

1.3.1 Timing Noise

Timing noise represents as a slow deviation in phase, frequency, or frequency derivative in various pulsars (Cordes & Downs, 1985; D'Alessandro, 1996; Hobbs, Lyne & Kramer, 2006). Fits by a simple spindown model show that the rms residuals are in a range of 7 orders of magnitude for various pulsars. A surplus of timing noise is observed in mag-

[3]The details for pulsar timing and other observing techniques can be found in Handbook of Pulsar Astronomy by Wright (2005)

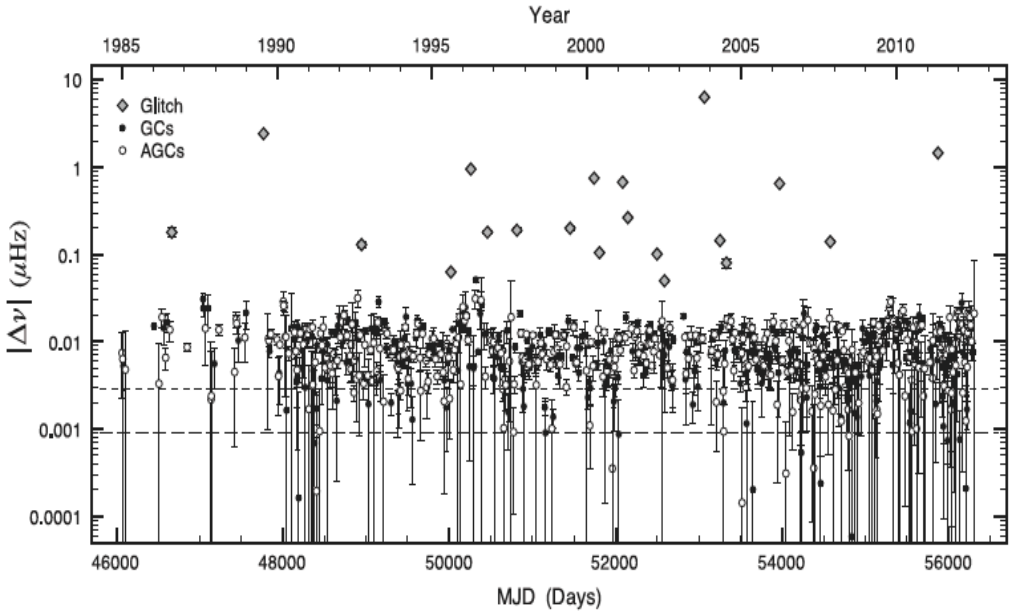

Figure 1.4: The glitch candidates of the Crab pulsar along the times. Horizontal lines show the limit of glitch detection. Figure Credit: Paper by Espinoza et al. (2014)

netars, whereas they are undetectable for most of milisecond pulsars. It is also suggested that there might be a correlation between the strength of timing noise and the magnitude of the spindown rate (Hobbs, Lyne & Kramer, 2010).

Although there is not a common explanation for this phenomena, there has been some attempts to clarify by different mechanisms, such as superfluid turbulence (Melatos & Link, 2014), changes in magnetospheric activity (Shemar & Lyne, 1996; Hobbs, Lyne & Kramer, 2010), and precession (D'Alessandro et al., 1993). The measurements of Lyne et al. (2010) for six pulsars point out that it can be also associated with pulse shape. There has been also some suggestions that timing noise might be caused by the glitches which are below the observational limits (Cheng et al., 1989, 1988). However the work of Espinoza et al. (2014) explored the group of small events (Figure 1.5) that are uncovered from timing noise and fitted as glitches. This gap between the measurements of timing noise and small glitch events suggest that there should be different mechanisms for these two phenomena[4].

[4]see chapter 3 for the details and some proposals for this distinction

1.3.2 Glitches

Glitches are sudden increases in the rotation rate of pulsars followed by relaxation towards the pre-glitch state. The fractional change of the angular velocity, $\Delta\Omega/\Omega$, in a glitch is in the range $\sim 10^{-11} - 10^{-5}$. Glitches are usually accompanied by jumps in the spin-down rate, $\Delta\dot{\Omega}/\dot{\Omega}$, in the range $\sim 10^{-4} - 10^{-2}$. To date, about 400 glitches have been observed in more than a hundred pulsars (Espinoza et al., 2011; Yu et al., 2013). It was showed by (Melatos, Peralta & Wyithe, 2008) that the size distributions of glitch events are fit with power laws with various indices from pulsar to pulsar, suggesting that they could be originated by self-organized critical processing, like quakes or vortex avalanches. Middle-aged pulsars, like Vela, exhibit glitch event the greatest in amount, while its activity and size decrease with age (Shemar & Lyne, 1996).

Glitch recoveries can distinguish in terms of their timescales (Figure 1.6). The characterized glitch parameters of $\Delta\nu$ and $\Delta\dot{\nu}$ can involve the permanent and/or decaying components. They have both the short-term relaxation, with characteristic time of hours to days, and the long-term relaxation, which is not sometimes observed due to being dominated by subsequent glitch. The abnormal glitch recoveries, usually correlated with the magnetospheric changes, have been also observed in the radio pulsars with high magnetic field such as PSR J1846-0258 (Livingstone, Kaspi & Gavriil, 2010), PSR J1718- 3718 (Manchester & Hobbs, 2011), PSR J1819-1458 (Lyne et al., 2009), and PSR J1119-6127[5] (Weltevrede, Johnston & Espinoza, 2011; Antonopoulou et al., 2015), and in magnetars, coexisting with some radiative changes like bursts (Kaspi & Gavriil, 2003; Kaspi et al., 2003; Dib, Kaspi & Gavriil, 2009).

Several models have been proposed to explain glitches and post-glitch relaxation. In the early starquake model (Ruderman, 1969), the solid crust of the neutron star occasionally cracks under stresses induced by the ongoing spin-down of the star, thereby readjusting to a less oblate shape closer to the equilibrium shape that a fluid star would follow while spinning down. By conservation of angular momentum, the reduction in moment of inertia of the crust is accompanied by an increase in its angular velocity. Glitches in the Crab pulsar (Wong, Backer & Lyne, 2001) and PSR J0537-6910 (Middleditch et al., 2006a) can be explained by this model. However, starquakes cannot explain large glitches that repeat every few years, as exhibited by the Vela pulsar (Baym & Pines, 1971). The required rate of dissipation of elastic energy stored in the solid crust would produce an X-ray luminosity enhancement which is not observed (Gürkan et al., 2000).

A second model is based on the relaxation towards the pre-glitch values on timescales

[5] see Chapter 1 for more details for this source

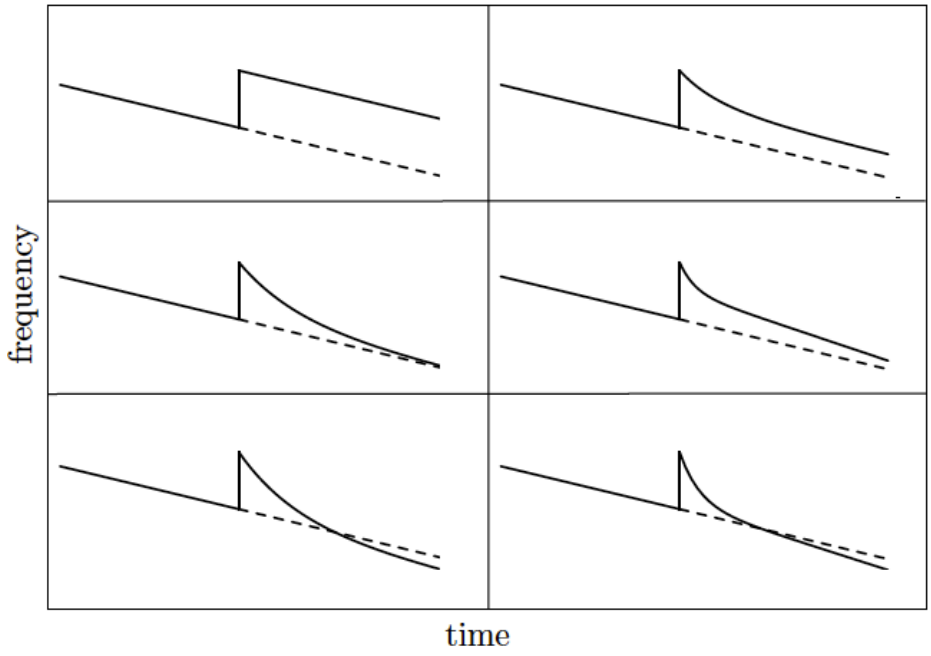

Figure 1.5: Schematic illustration of some typical glitch recoveries. Figure Credit: The Phd thesis of Danai Antonopoulou

of days to years, which is interpreted as a signature of superfluid interior components of the neutron star (Baym et al., 1969), as a star composed of normal matter would relax much faster. Anderson & Itoh (1975) proposed that interactions between quantized vortices, carrying the circulation of superfluid, and ions in the crustal lattice can regulate the outward motion of vortices. As the vortices are pinned by these interactions and the superfluid cannot spin down, storing angular momentum exhibits as glitches quasi-periodically.

The vortex creep model[6] (Alpar et al., 1984) is the most successful scenario in terms of explaining the large and frequent glitches, also the post-glitch behaviour of Vela and some other pulsars with structural parameters of neutron star (such as the inertial moment, temperature).

[6] see Chapter 1 for the details and formulation

Chapter 2

PECULIAR GLITCH OF PSR J1119-6127 AND EXTENSION OF THE VORTEX CREEP MODEL

This chapter was published in *Monthly Notices of the Royal Astronomical Society*, 2015, Volume 449, Issue 1, pp. 933-941

Onur Akbal, Erbil Gügercinoğlu, Sinem Şaşmaz Muş, and Mehmet Ali Alpar

2.1 Introduction

The 2007 glitch of PSR J1119-6127 is unusual and interesting as the first case with clear indications of changing pulsar emission properties coincident with the glitch. The event is also unusual in its long term signature of decreased spin-down rate. These signatures require an extension of the vortex creep model which has become the standard model for evaluating glitches and post-glitch response. The extension of the model must also make allowance for changes in the pulsar torque suggested by the glitch related changes in emission properties.

The standard model for the pulsar glitches is the vortex pinning−unpinning (vortex creep) model based on the dynamics of the neutron star's superfluid interior (Anderson & Itoh, 1975; Alpar et al., 1984). This model invokes the minimal storage and dissipation of energy for a star with angular momentum. The expected energy dissipation in a large glitch, at the expense of the rotational kinetic energies of the two components, does not violate any observational upper bounds. Models based on pinned superfluid components can explain the various modes of glitch and post-glitch behaviour (Haskell, Pizzochero & Sidery, 2012; Haskell & Antonopoulou, 2014).

Radio pulsar glitches observed up to the 2007 glitch of PSR J1119-6127 (Weltevrede, Johnston & Espinoza, 2011) showed no glitch correlated changes in the electromagnetic signatures, like pulse shape, emission pattern, spectrum and polarization. Previous applications of the vortex creep and starquake models assumed that there were no changes in the pulsar torque at the time of the glitch. Glitches and post-glitch response were explained entirely in terms of the internal structure and dynamics of the neutron star. The 2007 glitch of PSR J1119-6127 shows clear evidence for changing emission properties induced by the glitch, switching on intermittent pulses (see, e.g., Kramer et al., 2006) and also showing rotating radio transient (RRAT) behaviour (see, e.g., Keane & McLaughlin, 2011). Interestingly, this glitch also displayed $\Delta\dot{\Omega} > 0$ after transients have decayed, in contrast to the signatures of "standard" glitches which are characterized by a negative step in spin-down rate ($\Delta\dot{\Omega} < 0$). The high magnetic field radio pulsar PSR J1846-0258 had comparable glitch-induced emission changes (Livingstone, Kaspi & Gavriil, 2010). The radio pulsar PSR J0742-2822 showed a suggestive connection between changing radio emission and pulse shape features and glitch activity, however there is currently little direct evidence to establish a robust link between them due to absence of enough data following the glitch date (Keith, Shannon & Johnston, 2013). The RRAT J1819-1458 was also reported to have an increase in its activity associated with a glitch (Lyne et al., 2009).

In this paper we analyze the 2007 glitch of PSR J1119-6127 and extend the vortex

creep model to include the possibility of a sudden change in the pulsar torque associated with the glitch, as suggested by the changing emission properties, and to address the atypical glitch signature. In §2.2 we summarize the unique properties of the 2007 glitch of PSR J1119-6127. In §2.3 we review the vortex creep model, while in §2.4 we develop the model to include the unusual signatures in the spin frequency and spin-down rate, and allow for glitch associated changes in the pulsar torque. We apply our extended model to the peculiar glitch of PSR J1119-6127 in §2.5. We discuss our results in §2.6.

2.2 The Peculiar Glitch of PSR J1119-6127

PSR J1119-6127 is a young pulsar with a period $P = 0.41$ s and a period derivative $\dot{P} = 4 \times 10^{-12}$ Hz s^{-1} discovered by Camilo et al. (2000). It has a characteristic age $\tau_c \equiv P/(2\dot{P}) \cong 1625$ years, and a high surface dipole magnetic field $B \sim 8.2 \times 10^{13}$ G (at the poles). This pulsar has exhibited three glitches (Camilo et al., 2000; Weltevrede, Johnston & Espinoza, 2011). The third glitch, which occurred in 2007, was quite unusual in a number of ways (Weltevrede, Johnston & Espinoza, 2011):

1. For a while after the initial exponential relaxation is completed, the pulsar is found to be rotating with a smaller angular velocity as compared to the pre-glitch value, $\Delta\Omega(t) < 0$. In the latest data $\Delta\Omega(t) > 0$, and may be settling at a positive value (Antonopoulou et al., 2015).

2. In the long term, the pulsar slows down at a lower rate; the absolute value of the spin-down rate is less (the frequency derivative is greater) than its pre-glitch value, $\Delta\dot{\Omega} > 0$.

3. While the fractional changes in angular velocity are small, of the order of 10^{-9}, for the glitches of the Crab pulsar, Vela and older pulsars undergo large glitches of size $\Delta\Omega/\Omega \sim 10^{-6}$ as well as smaller "Crab-like" events. The 2007 glitch of PSR J1119-6127 is a "Vela-like" giant glitch from a young pulsar comparable to the Crab pulsar in characteristic age.

4. The radio emission properties of PSR J1119-6127 displayed changes associated with the glitch. The pulsar switched on intermittent pulses and also showed RRAT behaviour which seems to have emerged with the glitch. This anomalous emission behaviour of PSR J1119-6127 was observed for about three months following the 2007 glitch.

The much smaller second glitch which occurred in 2004 may have had similar signatures in the long term post-glitch frequency and frequency derivative remnants (Antonopoulou et al., 2015). The data is sparse, and post-glitch evolution may have been interrupted by the arrival of the 2007 glitch. Furthermore, no glitch associated changes in emission properties were observed for the 2004 glitch. Here we address only the 2007 glitch.

2.3 Overview of the Vortex Creep Model

The vortex creep model (Alpar et al., 1984; Alpar, Cheng & Pines, 1989) attempts to explain the processes which cause both the glitches and the post-glitch relaxation in terms of a number of distinct superfluid regions in the inner crust. The superfluid core of the neutron star is coupled to the external torque on very short timescales, via electron scattering off magnetized vortices (Alpar, Langer & Sauls, 1984). The core superfluid therefore behaves as part of the effective normal matter crust. Hence the superfluid component relevant for glitch and postglitch dynamics is the crust superfluid. A description of the core superfluid blue as well as the crustal superfluid in terms of mutual friction forces acting upon vortex lines is given by Andersson, Sidery & Comer (2006).

The dynamics of the crust superfluid is constrained by the pinning of the quantized vortex lines to nuclei, interstitial positions and possibly other structures in the crust lattice (Alpar, 1977; Link & Epstein, 1991; Mochizuki, Izuyama & Tanihata, 1999; Avogadro et al., 2008; Pizzochero, 2011; Haskell, Pizzochero & Sidery, 2012; Seveso et al., 2014). When vortices pin to nuclei, they move with the crust's velocity. A lag $\omega = \Omega_s - \Omega_c$ builds up between the superfluid and the crustal angular velocities Ω_s and Ω_c as the crust spins down under the external pulsar torque. This lag is sustained by the pinning forces acting upon the vortex line. In the case of rotational (cylindrical) symmetry, the magnitude of the required pinning force (per unit length) is $f = r\rho_s\kappa\omega = r\rho_s\kappa(\Omega_s - \Omega_c)$, where r is the distance from rotation axis, ρ_s is superfluid density, κ is the quantum of vorticity. The critical (maximum) lag, ω_{cr}, determined by the maximum available pinning force, is given by $\omega_{cr} = E_p/rb\rho_s\kappa\xi$. Here E_p is pinning energy, ξ is the vortex core radius and b is the distance between successive pinning sites along the vortex line. If local fluctuations in vortex density and superfluid velocity raise ω above ω_{cr}, there will be sudden unpinning and outward motion which can lead to an avalanche of vortex discharge (Anderson & Itoh, 1975). By conservation of angular momentum this leads to speeding up of the crust, $\Delta\Omega_c > 0$, observed as a glitch. The possibility of such vortex unpinning avalanches taking place spontaneously was confirmed by computer simulations (Melatos & Warszawski, 2009; Warszawski & Melatos, 2011; Warszawski, Melatos & Berloff, 2012).

Apart from the discontinuous angular momentum imparted to the crust by sudden vortex unpinning at glitches, the superfluid also spins down continuously between glitches by outward flow of vortices. The crustal neutron superfluid follows the spin-down of the crust by means of thermally activated outward creep of vortex lines against the pinning energy barriers (Alpar et al., 1984; Alpar, Cheng & Pines, 1989).

In terms of a simple two component model, involving the crust and the superfluid component, the observed spin-down of a neutron star's crust satisfies the equation,

$$I_c\dot{\Omega}_c = N_{ext} + N_{int} = N_{ext} - I_s\dot{\Omega}_s, \tag{2.1}$$

where $N_{ext} = I\dot{\Omega}_\infty$ is the external torque on the neutron star which tries to slow down the crust, and N_{int} is the internal torque arising from the coupling of the superfluid to the crust by vortex creep and tends to speed up the crust. I_c is the moment of inertia of the effective crust (including the superfluid core of the neutron star), I_s is the moment of inertia of the pinned superfluid, while their spin-down rates are $\dot{\Omega}_c$ and $\dot{\Omega}_s$, respectively. The spin-down rate $\dot{\Omega}_s$ of the superfluid is determined by vortex creep (Alpar et al., 1984). The system reaches a steady state when both the superfluid and the crust spin-down at the same rate $\dot{\Omega}_\infty \equiv N_{ext}/(I_s + I_c)$, sustained at the steady state lag ω_∞.

Glitches set the system off from steady state. Post-glitch relaxation is due to the recovery of vortex creep, as the lag ω inevitably builds back towards steady state due to the ongoing spin-down of the crust under the external pulsar torque. The internal torque is so sensitively dependent on the pinning energy E_p and the crustal temperature T that we expect vortex lines in the different regions of the superfluid to respond differently. Depending on the temperature and the local pinning parameters in relation to the external torque, vortex creep can have a linear or nonlinear dependence on the lag (Alpar, Cheng & Pines, 1989)[1]. In the linear regime, the response is linear in the glitch-induced perturbation to the lag ω and gives simple exponential relaxation. The relaxation time τ_l is very sensitively dependent on E_p/kT, with $\tau_l \propto exp(E_p/kT)$. The steady state lag $\omega_\infty = |\dot{\Omega}|_\infty\tau_l$ is always much less than ω_{cr} in this regime. From glitch observations, up to four exponential relaxation terms are seen from a particular pulsar (Dodson, Lewis & McCulloch, 2007).

In the opposite regime we have a very nonlinear response to perturbations. The re-

[1]The claim that the linear regime of vortex creep is never realized for realistic pinning parameters (Link, 2014) depends on the velocity of unpinned vortices, relying on the assumption that they move with the global averaged superfluid velocity with drag forces, and are not affected by the contributions of interactions with the adjacent pinning sites to the local superfluid velocity. This issue will be addressed in a separate work.

sponse of a nonlinear creep region k to the glitch will be (Alpar et al., 1984),

$$\Delta\dot{\Omega}_{c,k} = -\frac{I_k}{I}|\dot{\Omega}|_\infty \left[1 - \frac{1}{1 + (\mathrm{e}^{t_{0,k}/\tau_{nl}} - 1)\mathrm{e}^{-t/\tau_{nl}}}\right]. \tag{2.2}$$

At the time of glitch, creep in those regions which show nonlinear response can stop temporarily. These regions decouple from rest of the star, so that external torque acts on less moment of inertia. Creep restarts after a waiting time of $t_0 = \delta\omega/|\dot{\Omega}|_\infty$, since the external torque restores the glitch induced decrease in angular velocity lag. The relaxation time is

$$\tau_{nl} = \frac{kT}{E_p}\frac{\omega_{cr}}{|\dot{\Omega}|_\infty}.$$

In those superfluid regions through which the avalanche of vortices unpinned at the glitch pass, moving rapidly in the radially outward direction, the ensuing reduction $\delta\Omega_s$ in the superfluid rotation rate determines the offset $\delta\omega = \delta\Omega_s + \Delta\Omega_c$ in the lag, as $\delta\Omega_s \gg \Delta\Omega_c$. This results in the response given in Equation (2.2), characterized by the waiting time $t_0 \cong \delta\Omega_s/|\dot{\Omega}|_\infty > \tau_{nl}$. There can also be nonlinear creep regions through which no unpinned vortices pass at the glitch, so that $\delta\omega = \Delta\Omega_c$. In this case $t_0 = \Delta\Omega_c/|\dot{\Omega}|_\infty$ can be much shorter than τ_{nl}, and the contribution of such a nonlinear creep region reduces to simple exponential relaxation (Gügercinoğlu & Alpar, 2014),

$$\Delta\dot{\Omega}_{c,k} \cong -\frac{I_k}{I}\frac{\Delta\Omega_c}{\tau_{nl}}\mathrm{e}^{-t/\tau_{nl}} \tag{2.3}$$

like in the case of linear creep regions, but with the nonlinear creep relaxation time τ_{nl}.

If we integrate Equation (2.2) with the assumption that the post-glitch superfluid angular velocity decreases linearly in r over the region, corresponding to uniform density of unpinning vortices, one obtains (Alpar et al., 1984)

$$\frac{\Delta\dot{\Omega}_c(t)}{\dot{\Omega}_c} = \frac{I_A}{I}\left\{1 - \frac{1 - (\tau_{nl}/t_0)\ln\left[1 + (e^{t_0/\tau_{nl}} - 1)e^{-\frac{t}{\tau_{nl}}}\right]}{1 - e^{-\frac{t}{\tau_{nl}}}}\right\}. \tag{2.4}$$

In the limit $t_0 \gg \tau_{nl}$ this reduces to recovery with a constant $\ddot{\Omega}_c$

$$\frac{\Delta\dot{\Omega}_c(t)}{\dot{\Omega}_c} = \frac{I_A}{I}\left(1 - \frac{t}{t_0}\right), \tag{2.5}$$

as observed in the Vela pulsar (Alpar et al., 1993) and in most Vela-like giant glitches in older pulsars (Yu et al., 2013). In the above equations t_0 is the maximum waiting time, I_A is the moment of inertia of the vortex creep region A where unpinning of the vortices

has taken place during the glitch. Vortices unpinned in regions A pass through regions B with moment of inertia I_B before repinning in another creep region A. Regions B do not participate in spin-down by creep, as they do not sustain pinned vortices. Regions B contribute to the angular momentum transfer only at glitches, when an avalanche of unpinned vortices moves through them. These regions A and B determine the glitch, interglitch and long term behaviour of pulsars (Alpar et al., 1993, 1996).

After the exponential transients are removed, observable variables associated with glitches are related to the model parameters by the following simple three equations (Alpar & Baykal, 2006):

$$I_c \Delta\Omega_c = (I_A/2 + I_B)\delta\Omega_s. \tag{2.6}$$

$$\frac{\Delta\dot{\Omega}_c}{\dot{\Omega}_c} = \frac{I_A}{I}. \tag{2.7}$$

$$\ddot{\Omega}_c = \frac{I_A}{I}\frac{\dot{\Omega}_\infty^2}{\delta\Omega_s}. \tag{2.8}$$

Equation (2.6) simply states angular momentum conservation and gives the glitch magnitude. This is proportional to the number of vortices which participated in the glitch event. For a uniform array of vortices the number of unpinned vortices moving outward through radius r is related to the change in angular velocity of the superfluid at r,

$$\delta N = 2\pi r^2 \delta\Omega_s/\kappa \cong 2\pi R^2 \delta\Omega_s/\kappa, \tag{2.9}$$

since $r \cong R$, the radius of the star, in the crust superfluid. The angular momentum transfer depends on $\delta\Omega_s$ and the moment of inertia of the regions that vortices pass through, I_A and I_B. Equation (2.7) is about the torques acting on the pulsar. Before the glitch, in steady state, the crust superfluid and the rest of the star spin down at the same rate. When a glitch occurs, some part of the crustal superfluid decouples from the external torque leading to a jump in spin-down rate. Solving these equations for the three unknowns, I_A, I_B, and $\delta\Omega_s$, one can obtain model parameters uniquely without making any further assumptions.

2.4 Extension of the Vortex Creep Model

In the standard vortex unpinning-creep model only the outward motion of vortices is considered. This gives a negative post-glitch offset (an increase in the absolute value)

of the spin-down rate from its pre-glitch value, $\Delta\dot{\Omega} < 0$. The spin-down rate relaxes back to the pre-glitch value ($\Delta\dot{\Omega} \rightarrow 0$) for all modes of vortex creep which supply the internal torques from the superfluid acting on the normal matter crust. Thus, (i) glitches with the "wrong" sign in frequency and spin-down rate require inward vortex motion at the glitch; and (ii) long term (persistent) shifts in the spin-down rate require either a structural change in the neutron star crust, as proposed for the Crab pulsar (Alpar et al., 1996), or a glitch associated shift in the external torque (Link, Epstein & Baym, 1992).

Occasional inward fluctuations of vortices, facing an extra potential barrier, is a low probability component of the creep process. Therefore, bulk spontaneous inward motion of an avalanche of unpinned vortices is thermodynamically impossible in an isolated superfluid. Large numbers of vortices could be transported inward only if the glitch were induced by an agent external to the superfluid, like a starquake.

Inward vortex motion will increase the superfluid velocity by some $\delta\Omega'_s$ in regions of superfluid through which vortices have moved inward. Its effect can be investigated by changing t_0 with $-t'_0$, where $t'_0 \cong \delta\Omega'_s/|\dot{\Omega}|_\infty$. With this we obtain:

$$\Delta\dot{\Omega}_c = -\frac{I_{A'}}{I}|\dot{\Omega}|_\infty \left[1 - \frac{1}{1 + (\mathrm{e}^{-t'_0/\tau'_{nl}} - 1)\mathrm{e}^{-t/\tau'_{nl}}}\right], \tag{2.10}$$

where the primes indicate parameters associated with inward vortex motion. This equation describes the response to inward motion of unpinned vortices. When vortices travel inward, superfluid rotates faster. The lag ω thereby increases from its steady state value, and creep will be more efficient than in steady state, with an enhanced vortex current in the radially outward direction. If we integrate Equation (2.10) over a nonlinear creep region throughout which a uniform average density of vortex lines unpinned, or repinned, we obtain:

$$\frac{\Delta\dot{\Omega}_c(t)}{\dot{\Omega}_c} = \frac{I_{A'}}{I}\left\{1 - \frac{1 + (\tau'_{nl}/t'_0)\ln\left[1 + (e^{-t'_0/\tau'_{nl}} - 1)e^{-\frac{t}{\tau'_{nl}}}\right]}{1 - e^{-\frac{t}{\tau'_{nl}}}}\right\}. \tag{2.11}$$

The internal torque contribution given in Equations (2.10) and (2.11) leads to an initial positive contribution to $\Delta\dot{\Omega}_c$, which asymptotically decays to zero. Unlike the nonlinear creep response to glitch associated outward vortex motion, as given in Equation (2.2), the nonlinear creep response to inward vortex motion, does not have a waiting time. Instead Equations (2.10) and (2.11) display quasi-exponential relaxation. A constant second derivative $\ddot{\Omega}_c$ is not obtained from Equation (2.11) when $t'_0 \gg \tau'_{nl}$ or in any other limit. As the integrated response in Equation (2.11) is very similar, Equation (2.10) is adequate to describe the spindown rate when vortices have moved inward.

Allowing for the starquake induced inward vortex motion at the glitch, in addition to the natural outward motion of many unpinned vortices, we get the following equation instead of Equation (2.6),

$$I_c \Delta\Omega_c(0) = (I_A f + I_B)\delta\Omega_s - (I_{A'} f + I_{B'})\delta\Omega'_s. \tag{2.12}$$

where $f = 1/2$ is for the integrated response, Equations (2.4), (2.5) and (2.11), and $f = 1$ for the simpler response, Equations (2.2) and (2.10). The first term on the right hand side is the angular momentum transfer due to outward moving vortices, while the second term is the contribution of inward moving vortices. The physical meanings of $I_{A'}$ and $I_{B'}$ are similar to their non-primed counterparts. A plate of the crustal solid that moves inward in a quake could carry vortices with it, in the inward, $-r$, direction. Nonlinear creep regions with moment of inertia $I_{A'}$, and vortex free regions with moment of inertia $I_{B'}$ are at radial positions between the original and the new positions of the plate, and therefore experience a sudden increase $\delta\Omega'_s > 0$. As creep relaxes back to steady state, the net angular momentum transfer from the regions A and A' is zero, while the regions B and B' transport angular momentum only at glitches and will contribute a remnant frequency offset $\Delta\Omega_p$:

$$I_c \Delta\Omega_p = I_B \delta\Omega_s - I_{B'} \delta\Omega'_s. \tag{2.13}$$

Extending Equation (2.7) to describe the net glitch in the spin-down rate with the terms of opposite signs describing the response of creep to outward and inward vortex motion, we obtain

$$\frac{\Delta\dot{\Omega}_c}{\dot{\Omega}_c} = \frac{I_A}{I} - \frac{I_{A'}}{I}. \tag{2.14}$$

For PSR J1119-6127 the post-glitch $\Delta\dot{\Omega} > 0$ persists for ~ 2500 days, as far as the pulsar has been observed since the glitch (Antonopoulou et al., 2015). Here we pursue the assumption that $\Delta\dot{\Omega}_c > 0$ is permanent; that it will not decay on long timescales in the future. This is a viable assumption with the present data, as discussed in the next section. With this assumption the permanent shift $\Delta\dot{\Omega}_p$ could be due to a structural change in the star, as postulated for the persistent shifts in spin-down rate observed to accompany the Crab pulsar glitches (Alpar et al., 1996), or, alternatively, due to a glitch associated permanent change in the external torque. Unlike the Crab pulsar, the 2007 glitch of PSR J1119-6127 has strong indications that actually the external torque has changed, since the pulsar has switched to intermittent and RRAT behaviour with the glitch. It is likely that structural changes experienced by PSR J1119-6127 lead to a permanent change in the

external torque.

2.5 Model Fits

We apply a model which is an extension of earlier applications of the vortex creep model to the Vela (Alpar et al., 1993) and Crab (Alpar et al., 1996) pulsars' glitches. We take one nonlinear creep region with relaxation time τ_2 corresponding to the outward motion of the glitches. The new component in the extended model is the inclusion of inward moving vortices in the glitch, which move through a nonlinear creep region with relaxation time τ_1 (cf. Equation (2.10)). We also employ a region in which relaxation occurs exponentially with a timescale τ_3, discussed below. Finally, we include a possible external torque change as a constant offset to the spin-down. We tried model fits with the integrated response, Equations (2.4) and (2.11) and with the simple response Equations (2.2) and (2.10). As the residuals are comparable, we choose to employ the simple model.

The expression used for the fit including our extended formula is:

$$\begin{aligned}\Delta\dot{\Omega}_c(t) = &- a_1\left[1 - \frac{1}{1+\alpha_1 e^{-(t+\Delta)/\tau_1}}\right] \\ &- a_2\left[1 - \frac{1}{1+\alpha_2 e^{-(t+\Delta)/\tau_2}}\right] - a_3 e^{-(t+\Delta)/\tau_3} + b. \end{aligned} \tag{2.15}$$

The various parameters are defined by: $a_1 = \frac{I_{A'}}{I}|\dot{\Omega}|_\infty$, $a_2 = \frac{I_A}{I}|\dot{\Omega}|_\infty$, $\alpha_1 = (e^{-t_0'/\tau_1} - 1)$, $\alpha_2 = (e^{t_0/\tau_2} - 1)$, $a_3 = \frac{I_3}{I}\frac{\delta\omega}{\tau_3}$, and $b = (\Delta N_{ext}/N)\dot{\Omega}_\infty$, and t is the time since the first post-glitch observation, with the time lag Δ between the actual glitch date and the first post-glitch observation. We have 9 free parameters. Parameters with the subscript "1" denote the contribution from the response of vortex creep to glitch associated inward vortex motion, while those with subscript "2" and "3" are associated with creep response to glitch associated outward vortex motion.

The exponential relaxation term with amplitude a_3 might describe the response of either an intrinsically linear creep region, or a nonlinear creep region where there was no vortex motion at the glitch, so that the angular velocity of the superfluid remains unchanged and the glitch induced perturbation to the angular velocity lag is simply $\delta\omega = \Delta\Omega_c$ (Gügercinoğlu & Alpar, 2014). We adopt the latter interpretation. This assumption is consistent with the results obtained from the fits.

The moments of inertia of nonlinear creep regions contributing to the long term response are obtained from the fit parameters a_1 and a_2. The terms α_1 and α_2 yield the numbers of vortices moving inwards and outwards, respectively, during the glitch. b is the long term offset of $\Delta\dot{\Omega}_c$ after all the contributions from creep regions relax back to

zero. We interpret this as the contribution of the change in the external torque. The terms with subscripts "2" and "3" contribute $\Delta\dot{\Omega}_c(t) < 0$ while the parameter b (external torque change) and the term with subscript "1" (inward motion of vortices) contribute $\Delta\dot{\Omega}_c(t) > 0$ (see Figure 2.1). This term has the longest time constant, $\tau_1 \gg \tau_2 > \tau_3$. The data could also be fitted by assuming no change in the external torque, $b = 0$ and choosing long enough τ_1 so that in the long run $\Delta\dot{\Omega}_c$ relaxes back to zero while accommodating the $\Delta\dot{\Omega}_c(t) > 0$ values for the latest present observations. We have explored models with $0 \leq b \leq 1.1 \times 10^{-13}$ rad s^{-2}, corresponding to $-7.2 \times 10^{-4} \leq N_{ext}/N \leq 0$. The values of b between 0.8×10^{-13} rad s^{-2} and 1.1×10^{-13} rad s^{-2} yield reasonable fit results. Here we choose to explore the possibility of a permanent change in the external torque as reflected by $b = 1 \times 10^{-13}$ rad s^{-2}. However, at present we cannot rule out $b = 0$, a full decay. Parameters of the best fits with $b = 0$ and $b = 1 \times 10^{-13}$ rad s^{-2} are shown in Table 2.1. The long term data display quasi-periodic residuals with a period of $\sim$ 400 days (Antonopoulou et al., 2015); we find a best fitting sinusoidal period $P = 394$ d by fitting the data from the last $\sim$1500 days with a model involving only the terms that are dominant in the long term: the contributions from inward moving vortices, the long-term offset with $b = 1 \times 10^{-13}$ rad s^{-2} and the sinusoidal term. In our further investigations comprising all the data we fixed this period for the sinusoid. The residuals of the $b = 1 \times 10^{-13}$ rad s^{-2} model also show initial fluctuations, which may be due to transient emission patterns in the magnetosphere. Future timing data will distinguish between these alternatives.

To apply our extended creep model to the peculiar glitch of PSR J1119-6127, we use the spin-down rate data for the 2007 glitch, a total of 85 data points. The arrival time data from MJD 54268 indicate that a glitch has taken place since the previous data set on MJD 54220. The first post-glitch data fit to produce frequency derivative values is dated MJD 54300 (Weltevrede, Johnston & Espinoza, 2011). The presently available spin-down rate and frequency data extending to MJD 56751 was kindly shared with us by Patrick Weltevrede (P. Weltevrede private communication, Antonopoulou et al. (2015)). The time interval Δ between the actual glitch date and the first post-glitch frequency derivative values thus lies between $\Delta = 32$ days and $\Delta = 80$ days. The coefficient I_3/I of the exponentially relaxing term is sensitive to the choice of Δ. We arbitrarily take $\Delta = 60$ days, which gives $I_3/I \cong 1.74 \times 10^{-1}$.

We use the Levendberg-Marquardt method to find the best fit values of the parameters, starting from initial guesses with MPFITFUN procedure (Markwardt, 2009)[2]. The best fit is displayed in Figure 2.1 and its parameters are listed in Table 2.1. Inferred model parameter values corresponding to Equation (2.15) are shown in Table 2.2.

[2]http://purl.com/net/mpfit

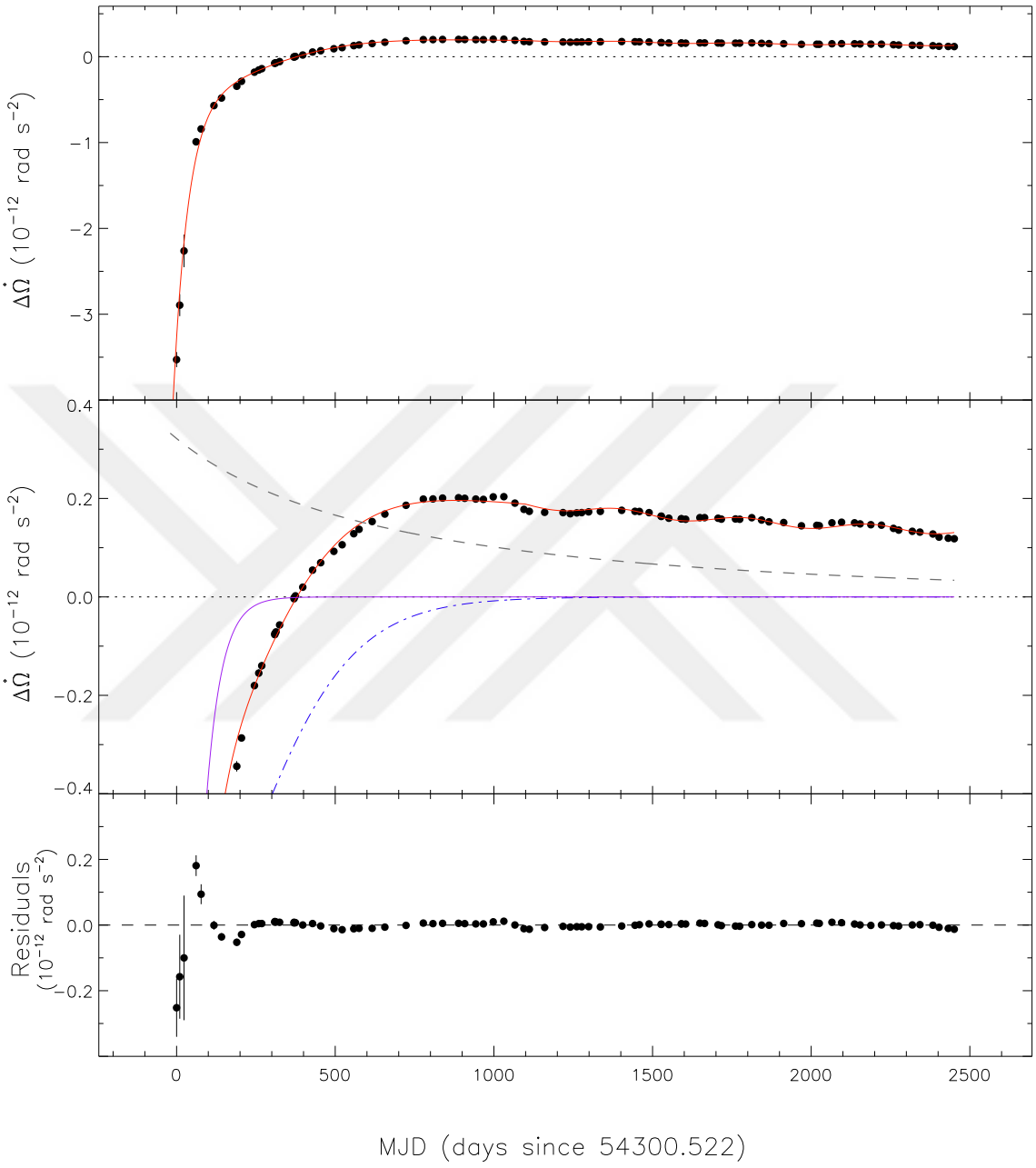

Figure 2.1: Top panel: Fit to the post-glitch spin-down rate data with the model of Equation (2.15), with $\Delta = 60$ days and b = 1.0×10^{-13} rad s^{-2}. Middle panel: Zoomed version of top panel with model components representing contribution of exponential relaxation term (purple solid line), inward moving vortices (gray dashed line) and outward moving vortices (blue dash dotted line) are shown separately. Sinusoidal component and long-term offset b are not shown in the figure for clarity. Bottom panel: Difference between data and model.

Table 2.1: Parameters of the best fits to the postglitch frequency derivative data following the 2007 glitch of PSR J1119-6127, with $\Delta = 60$ days, and $b = 1.0 \times 10^{-13} rad\ s^{-2}$ (first column) and $b = 0$ (second column)

Parameter	Value (Error)	Value (Error)
$(a_1)_{-13}(rad\ s^{-2})$	1.68 (0.77)	0.34 (0.29)
$(a_2)_{-13}(rad\ s^{-2})$	10.16 (1.43)	5.93 (0.39)
$(a_3)_{-12}(rad\ s^{-2})$	9.92 (0.55)	8.01 (0.38)
α_1	-0.68 (0.15)	-0.90 (0.07)
α_2	6.34 (1.48)	20.65 (3.82)
$\tau_1(days)$	1796 (211)	20475 (14413)
$\tau_2(days)$	159 (7)	129 (4)
$\tau_3(days)$	48 (2)	58 (2)
$(b)_{-13}(rad\ s^{-2})$	1.0	0.0

Table 2.2: Inferred Parameters with $b = 1.0 \times 10^{-13} rad\ s^{-2}$.

Parameter	Value
$\left(\frac{I_{A'}}{I}\right)_{-3}$	1.11
$\left(\frac{I_A}{I}\right)_{-3}$	6.70
$\left(\frac{I_3}{I}\right)_{-1}$	1.74
$t'_0(days)$	2046
$t_0(days)$	317
$(\delta\Omega')_{-2}\,(rad\ s^{-1})$	2.69
$(\delta\Omega)_{-3}\,(rad\ s^{-1})$	4.16
$\left(\frac{\Delta N_{ext}}{N}\right)_{-4}$	-6.58

The long term remnant $\Delta\Omega_p$ of the glitch in frequency can be found by comparing the indefinite integral of the model for spin-down rate with the observed frequency residual at the latest available data points. Using the frequency residual data on MJD 56688, $\Delta\Omega_p \cong 9.4 \times 10^{-5}$ rad s^{-1} is obtained. We find $\Delta\Omega_p > 0$, unlike the earlier result of Weltevrede et al. (2011), who found a negative long term frequency residual based on the latest post-glitch data then available, but in agreement with their current estimate (Model A in Antonopoulou et al. (2015)).

2.6 Discussion and Conclusions

We have examined the peculiar 2007 glitch of PSR J1119-6127 by extending the vortex creep model to take into account (i) the possibility of a glitch associated change in the pulsar external torque, and (ii) inward motion of vortices. Both of these effects can be induced by a starquake that triggered the glitch. We model the peculiar glitch of PSR J1119-6127 as follows: a crustquake occurs, causing the crustal plates to move towards the rotation axis, together with some pinned vortices. At the same time, some vortices affected by the crustquake are unpinned and move outward. The glitch is due to the angular momentum transfer associated with the sudden outward and inward vortex motions. Magnetic field lines, which move with the conducting crustal plate, change the external torque and give rise to the abnormal emission properties.

In contrast to the changes in other pulsars' glitches, the long-term change in spin-down rate, after transients are over, is (possibly) positive for PSR J1119-6127. In the creep process under the action of an external spin-down torque, the inward motion of vortices is thermodynamically unlikely, unless induced by a driving force such as arising from crustquake induced motion of crustal plates that carrying pinned vortices inwards. Inward vortex motion increases the lag between local superfluid and normal matter rotation rates from the steady state value, thereby accelerating rather than cutting off the creep process. This in turn increases the rate of angular momentum transfer to the crust and thereby decreases the spin-down rate of the crust, producing a positive change in the observed crust spin-down rate. By contrast, in standard glitches vortices move outward, decreasing the lag and turning off or suppressing the creep process which transfers angular momentum from superfluid to the crust; this leads to a negative step in the spin-down rate of the crust. Glitch induced steps of either sign arising from the offset in the vortex creep process always relax back to the pre-glitch spin-down rate as the creep process heals back to the steady state. The model we have fitted to the spin-down rate data after the 2007 glitch of PSR J1119-6127 includes the creep response to outward and inward

vortex motion as well as a glitch associated change in the external (pulsar) torque.

Antonopoulou et al. (2015) fit their data set with two models, model A with a long term exponential relaxation, and model B with a negative frequency second derivative ($\Delta\ddot{\nu}_p < 0$ in their notation). The positive $\Delta\dot{\Omega}_c$ decays towards zero in both models, asymptotically in the case of Model A. The two models leave comparable residuals. Our investigation of crust breaking, giving a permanent change in the external torque and spin-down rate and causing inward vortex motion, is complementary to their work. Future timing observations will decide if the offset in the spin-down rate is really permanent or relaxing; and searches for thermal signals accompanying future glitches of PSR J1119-6127 will distinguish between the different models.

We must use the long term remnant of the frequency glitch in Equation (2.13) to constrain I_B and $I_{B'}$, the moments of inertia of superfluid regions which transfer angular momentum only at glitches, due to the outward and inward motion of unpinned vortices, respectively. Using the values of $\delta\Omega_s$ and $\delta\Omega'_s$ from Table 2.2 leads to the constraint $9.4 \times 10^{-5} I = 4.2 \times 10^{-3} I_B - 2.7 \times 10^{-2} I_{B'}$. This gives $I_B/I > 2.2 \times 10^{-2}$. Then the superfluid creep regions with a total moment of inertia $I_s > I_A + I_B + I_{A'} + I_{B'} + I_3 > I_A + I_B + I_{A'} + I_3 \gtrsim 20.4 \times 10^{-2} I$ is effected by the glitch event. The region with moment of inertia $I_3 = 1.74 \times 10^{-1} I$ comprises most of the moment of inertia in pinned superfluid.

Recent calculations (Chamel, 2013; Andersson et al., 2012) show that Bragg scattering of conduction neutrons from nuclei in the neutron star crust induces a neutron effective mass that is larger than the bare mass. This "entrainment" of superfluid neutrons in the crust by the crystal lattice requires that the actual moment of inertia associated with the superfluid response is larger by a factor $m_n^*/m_n > 1$ where m_n^* and m_n are effective and bare neutron masses in the lattice. The moment of inertia $I_s \gtrsim (m_n^*/m_n)\, 20.4 \times 10^{-2} I$ associated with creep cannot be accommodated by the crust superfluid alone for most neutron star models, even without the effective mass correction. In addition to the crust superfluid, other locations are required to sustain vortex creep. Contribution from vortex line-toroidal flux line pinning and creep at the outer-core of the neutron star (Sidery & Alpar, 2009), which has a comparable or larger moment of inertia than that of the crust superfluid, could provide the required extra moment of inertia (Gügercinoğlu & Alpar, 2014). The moment of inertia of the creep region where vortex motion is controlled by the toroidal arrangement of flux lines can amount to $I_{\rm tor}/I \sim 2 \times 10^{-1}$ depending on the radial extension of the toroidal field in the outer core. Creep here is in the non-linear regime. As no glitch associated vortex motion is expected, the response to a glitch is exponential relaxation (Gügercinoğlu & Alpar, 2014). The relaxation time $\tau_{\rm tor} \cong 50$ days

for PSR J1119-6117 parameters is in line with our estimate of $\tau_3 \cong 48$ days (and with $\tau_{nl} \cong 33$ days for the application to the Vela pulsar, which has parameters similar to those of PSR J1119-6117; Gügercinoğlu & Alpar (2014)). So, we argue that $I_3/I = 1.74\times10^{-1}$ reflects the moment of inertia associated with the toroidal flux line region of the outer core. The moment of inertia of the crustal superfluid participating in the glitch, when the crustal entrainment correction is included, is $I_{s,\rm crust} > (m_n^*/m_n)(I_A + I_B + I_{A'}) \gtrsim (m_n^*/m_n)\ 2.98 \times 10^{-2} I$. This total moment of inertia fraction can be accommodated in the crust in neutron star models with hard equations of state, if the mean value of m_n^*/m_n to represent the crust superfluid is not much larger than 1. The recent work of Piekarewicz, Fattoyev & Horowitz (2014) shows that the neutron star crust may maintain larger moment of inertia so that the above constraint is easier to be satisfied.

The total numbers of vortices displaced in this glitch are determined by the superfluid angular velocity changes $\delta\Omega_s$ and $\delta\Omega_s'$ using Equation (2.9). The number of vortices that have moved outward is found to be is $\delta N_{out} \sim 1.3\times10^{13}$, while the corresponding number for inward moving vortices is $\delta N_{in} \sim 8.4 \times 10^{13}$. These numbers are typical of all small or large glitches, from Crab, Vela and other pulsars analyzed so far in terms of vortex unpinning, indicating a particular scale of the glitch trigger.

The glitch associated change in the external torque contributes a constant offset from the pre-glitch behaviour that remains in the spin-down rate after all post-glitch relaxation is over. This term, denoted b in Equation (2.15), indicates a change in the external torque, which leads to a change in the spin-down rate through $\Delta N_{ext}/N_{ext} = \Delta\dot{\Omega}/\dot{\Omega} + \Delta I/I$. The actual fractional change in the moment of inertia associated with a possible quake must be less than the observed glitch magnitude, so $|\Delta I/I| < \Delta\Omega/\Omega \sim 10^{-5} << |\Delta\dot{\Omega}/\dot{\Omega}| \sim 10^{-4}$. The measured permanent term b in $\Delta\dot{\Omega}/\dot{\Omega}$ therefore gives the fractional change in the external torque. Taking the external torque to be essentially the dipole radiation torque, we have:

$$\frac{\Delta N_{ext}}{N_{ext}} = 3\frac{\Delta\Omega_c}{\Omega_c} + 2\frac{\Delta B_\perp}{B_\perp} \cong 2\frac{\Delta B_\perp}{B_\perp}, \tag{2.16}$$

as the term $3\Delta\Omega_c/\Omega_c \sim 10^{-5}$ is again negligible. We assume that the magnetic field change is associated with crust breaking, involving broken plates of size D distributed in a ring of the crust of width D and radius $R\cos\alpha$ from the rotation axis, with each plate moving a distance D at the quake. The field moves with each broken piece of the conducting crust, without any change in the local field magnitude, and orientation, which we take to be normal to the crust plate. The local field strength varies azimuthally in the broken ring. We further assume that the broken ring is in the polar regions of the magnetic field, so that the crust breaking has a strong effect on the external torque. This assumption

is plausible if magnetic stresses play a role in crust breaking (Franco, Link & Epstein, 2000; Lander et al., 2015). A schematic view of our model for external torque variation via change of magnetic field's perpendicular component is depicted in Figure 2.2. The external torque variation is related to the change $\Delta\alpha$ in the angle between the rotation and magnetic axes:

$$\frac{\Delta B_{\perp}}{B_{\perp}} = \frac{\Delta\alpha}{\tan\alpha}. \tag{2.17}$$

From our estimate of the change in external torque, $\Delta N_{ext}/N_{ext} \cong -6.58 \times 10^{-4}$ given in Table 2.2, we obtain:

$$\Delta\alpha = \frac{1}{2}\frac{\Delta N_{ext}}{N_{ext}}\ \tan\alpha \cong (-3.3 \times 10^{-4})\ \tan\alpha \tag{2.18}$$

which is between (-1.0×10^{-4}) and (-2.8×10^{-4}). To obtain this, we have used the range of α considered by Weltevrede, Johnston & Espinoza (2011), $\alpha \sim 17^\circ - 30^\circ$ corresponding to an emission height ~ 500 km and $\alpha \sim 30^\circ - 40^\circ$ corresponding to an emission height ~ 1800 km. The tiny change $\Delta\alpha$ in inclination angle cannot be resolved as an observable glitch associated pulse shape change in the present radio timing data. Motion of crustal plates towards the pole ($\Delta\alpha < 0$) results in a reduction in the moment of inertia of the solid, and therefore an increase in the spin-down rate. This is the signature of a crust quake in a spinning down pulsar, tending to make the shape more spherical. The reason for the external torque change is likely to be a starquake, inducing motion of crustal plates, and reducing $B_{\perp}$, as the surface magnetic field moves with the conducting plates towards the rotation axis.

The fractional change in moment of inertia due to the motion of the crustal plates is $\Delta I/I \sim (m/M)\Delta\alpha \lll \Delta\alpha \sim 10^{-4}$, where m is the total mass of the moving plates and M is the mass of the entire star. Observing the direct effect of this actual change in the crustal moment of inertia as a glitch is impossible. The glitch magnitude $\Delta\Omega$ is due to amplification by the vortex motion triggered by crust-breaking and the resulting angular momentum transfer from superfluid to normal matter. We have assumed that some of the vortices pinned to the moving plates are initially carried inward with the plates. This is possible when the increase $\delta\Omega'$ in superfluid rotation rate, due to the inward motion of the pinned vortices on the time scale of crust breaking is not sufficient for the local lag to increase from the steady state value to the critical value, $\delta\Omega' < \omega_{cr} - \omega_{\infty}$, for typical values of ω_{∞} (Alpar, Cheng & Pines, 1989). These vortices will bend and are likely to be strongly perturbed by the sudden inward motion and become unpinned. The unpinned vortices will then move downstream azimuthally with the superfluid flow, causing more

vortices to unpin and scatter outward until they reach a new radial position where they join the background vortex flow and creep. The avalanche of unpinning takes place rapidly on the glitch "rise" timescale. Some number δN_{in} of vortices associated with the moving plates end up in radial positions inward of their original position while a number δN_{out} of vortices end up in radial positions further out compared to their original position. The moment of inertia of the superfluid creep regions affected by the inward motion of the plates and net inward vortex motion is of order

$$I_{A'}/I \cong \frac{4\pi\rho_s R^4 D \sin\alpha\cos^2\alpha}{(2/5)MR^2} \simeq 15/2 \sin\alpha\cos^2\alpha\,(D/R)$$
$$\sim (2D/R), \tag{2.19}$$

assuming a uniform density neutron star, and adopting $\sin\alpha\cos^2\alpha \cong 0.3$ for the range of $\alpha \cong 17^\circ - 40^\circ$ indicated by Weltevrede, Johnston & Espinoza (2011). Using the value of $I_{A'}/I$ from fits, we obtain the ring width $D \sim 6R_6$ m, where R_6 is the neutron star radius in units of 10^6 cm. The number of vortices pinned to each plate is

$$\delta N_{plate} \sim D^2 \frac{2\Omega}{\kappa} \sim 3 \times 10^8 \Omega R_6^2 \sim 5.5 R_6^2 \times 10^9. \tag{2.20}$$

The total number of vortices associated with broken plates with a net inward motion during the glitch, is $\delta N_{in} \sim 8.4 \times 10^{13}$ vortices, as we estimated above from the results of our fits for t_0', a parameter independent from $I_{A'}/I$ which we used to estimate the plate size D. The number of plates involved should be $\sim \delta N_{in}/\delta N_{plate} \sim 10^4$, in agreement with the number of plates in the broken ring, $\sim 2\pi R/D \sim 10^4$. A comparable number of vortices $\delta N_{out} \sim 1.3 \times 10^{13}$ end up moving outward through a superfluid region of comparable moment of inertia, I_A. We find here an indication that the common scale, $\sim 10^{13}$, of the number of vortices unpinned in all pulsar glitches may be associated with the number of vortices in the typical plate size D involved in a triggering crust quake, multiplied by the number of plates involved, $\sim 2\pi R/D \sim 10^4$. These scales rest on the single parameter, the plate size D which must be related to the physics of the crustal solid. This plate size D is of the same order of magnitude as the 'mountain' height ~ 1 m estimated for the Crab pulsar (Chamel & Haensel, 2008). Note that the critical strain angle θ_{cr} at which the crust lattice breaks is $\theta_{cr} \sim D/h$ where h is the radial thickness of the broken crustal plates. Thus,

$$\theta_{cr} \sim 10^{-2} \left(\frac{D}{1\ m}\right) \left(\frac{h}{100\ m}\right)^{-1},$$

compatible with the results of Horowitz & Kadau (2009) for the critical strain angle.

It is interesting to compare the moment of inertia fractions in crust superfluid regions

through which the unpinned vortices moved during the peculiar glitch of PSR J1119-6127, given in Table 2.2, with the corresponding Crab (Alpar et al., 1996) and Vela (Alpar et al., 1993) values, $(0.01 - 1.87) \times 10^{-3}$ and $(2.3 - 3.4) \times 10^{-2}$ respectively, as this gives a lower limit on the moment of inertia fraction in the crust, leading to constraints on the neutron star equation of state (Datta & Alpar, 1993; Link, Epstein & Lattimer, 1999). With its characteristic age of $\sim$ 1625 years, PSR J1119-6127 is between the Crab and Vela pulsars in age, but its implied crustal superfluid moment of inertia fraction 2.98×10^{-2} is comparable to the values inferred for the Vela pulsar. The qualitative evolution of glitching behaviour from Crab-like to Vela-like was proposed to be due to the development of connections in a network of vortex creep regions, so that the moment of inertia involved increases with age (Pines & Alpar, 1985). PSR J1119-6127 should already have a sufficiently well connected vortex creep network. Presumably the high magnetic field and associated stresses in the crust of this pulsar lead to high crust breaking activity. While similar moments of inertia in vortex creep regions I_A are inferred, and the long term fractional offsets in the spin-down rate are similar in absolute value, for the Crab case no change in electromagnetic signature is observed.

Magnetic stresses will play a role comparable to that of rotation induced stresses in conventional starquake models if, roughly,

$$\frac{B_0^2 - B^2}{8\pi} \sim \frac{1}{2}\rho R^2 \left(\Omega_0^2 - \Omega^2\right) \sim \frac{1}{2}\rho R^2 \Omega \mid \dot{\Omega} \mid t_g,$$

where B_0 and Ω_0 denote reference values of B and Ω frozen into the crust. Using the glitch interval $t_g \sim 3$ yrs, typical for young pulsars, we find that magnetic stresses can play a role where $B \gtrsim 10^{13}$ G in the crust. The magnetic field can have poloidal and toroidal components whose geometry will determine where in the crust the local stresses reach the critical values for crust breaking (Lander et al., 2015). The higher multiple components of the magnetic field and the geometry of the stress tensor when both magnetic and rotational effects are included further complicate the situation. In addition, the changes in electromagnetic signature, as seen only in PSR J1119-6127, are likely to occur if the broken plate extends to the surface and leads to reconfiguration of the magnetosphere. This may explain why the behaviour exhibited by PSR J1119-6127 is rare. As a rough guideline, such behaviour may be exhibited by young pulsars with high magnetic field in young pulsars with high magnetic field.

We should note the different responses of the crust and the superfluid to a starquake. After the crust breaks and plates move towards the rotation axis in order to relieve their stresses, those broken pieces of the crust are stuck to new metastable positions, and do not come back to their pre-glitch sites. Thus, crust breaking and crustal motion are irre-

versible. Starquake induced inward motion of vortices leads to a local excess of vortex lines and thereby to faster rotation of the superfluid. Creep becomes more efficient, evolving back towards steady state with an enhanced vortex current, as described by the vortex creep response employed in our fits. In the end, the superfluid relaxes back to the pre-glitch dynamical steady state, and all the parts of crustal superfluid and the rest of the star spin-down at the same rate. Indeed, without structural changes, the response of all internal torques will always relax back to $\Delta\dot{\Omega}_c = 0$.

The main reason of the switch in emission patterns to intermittent and RRAT behaviour lasting for about a hundred days after the event in 2007 is likely to be the effect of the quake on magnetic field lines which are anchored to the crust. If the magnetospheric field pattern could move rigidly, without distortion, together with the motion of the crustal plate, as a consequence of the shift by $\Delta\alpha \sim 10^{-4}$, there would be no significant change in the emission pattern. However, when a crustal plate moves in a quake, the elastic response of the field lines, which twist and reconnect, can amplify a small shift in the crustal position into a complex and drastic change in the emission pattern, helped by rotation which results in twisting of magnetic field lines anchored to the highly conducting crust (Beloborodov, 2009). The distorted magnetospheric geometry will subsequently relax towards a quasi-stable configuration for the new position of the plate. The changes in the emission pattern are observed for about a hundred days following the glitch, after which the pulsar returns to its pre-glitch pulse shape and emission pattern. Twisting of field lines and their subsequent relaxation will also introduce temporary fluctuations in arrival times. Our timing model fits indeed leave relatively large residuals for about a hundred days in the post-glitch data given in the bottom panel of Figure 2.1.

Although the recently discovered magnetar anti-glich from 1E 2259+586 by Archibald et al. (2013) has also shown a negative spin jump and changing emission features, the situation is very different from that of PSR J1119-6127. In the case of 1E 2259+586, the magnitude of the change in spin-down rate, $|\Delta\dot{\Omega}| \sim 2.8|\dot{\Omega}|$ is too large to be associated with the superfluid regions in the star. It is likely that only a large change in the external torque is involved, as suggested by the violent change in emission, so that this magnetar 'antiglitch' must be external/magnetospheric in origin (Lyutikov, 2013; Tong, 2014).

In summary, the peculiar glitch of PSR J1119-6127 offers an invaluable opportunity for the reexamination and extension of glitch models to account for anomalous glitch signatures and transient emission phenomena initiated by a quake leading to a change in the external torque and triggering the response of the superfluid regions of the neutron star. Our model predicts that the change in the external torque is permanent. The coincidence of the numbers of vortices involved in the glitch with the numbers inferred in Crab and

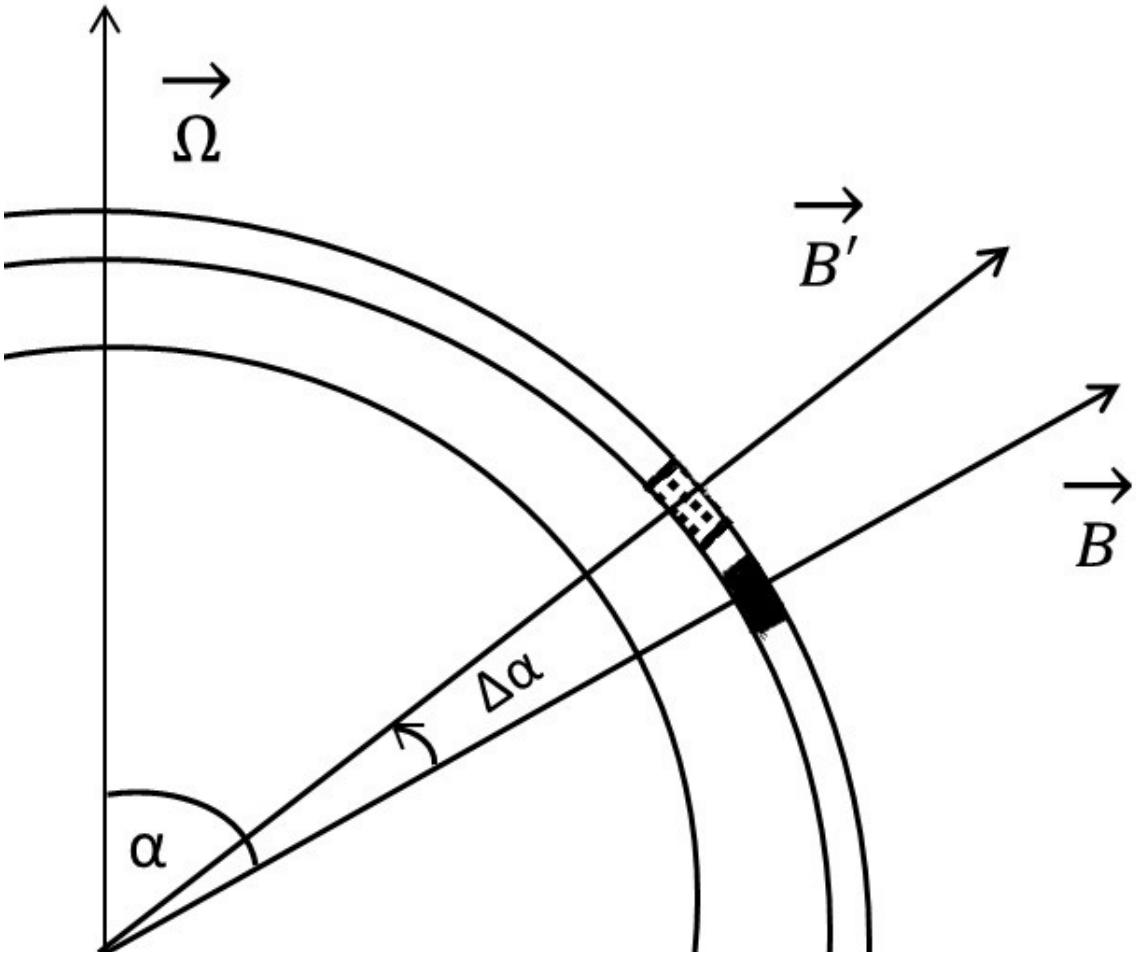

Figure 2.2: Starquake Model in cross section. The dotted area represents new position of crustal plates (broken ring) after the starquake.

Vela pulsar glitches is highly suggestive, supporting the explanation in terms of a crust breaking event with a typical plate size, which may be a common, even universal, trigger for glitches. If future timing observations rule out a permanent change in the external torque, this coincidence would turn out to be spurious. The explanation of the post-glitch evolution of $\Delta\dot{\Omega}_c(t)$ in terms of internal torques responding to glitch associated inward and outward vortex motion, and relaxing to $\Delta\dot{\Omega}_c = 0$ is viable when there are no observed changes in the external torque.

Chapter 3

Interglitch Time Intervals of the Vela Pulsar

3.1 Introduction

The Vela pulsar, PSR 0833-45, is the most productive and engrossing source in terms of the glitch events, having provided us with 16 large glitches with mostly $\Delta\Omega/\Omega \sim 10^{-6}$ and $\Delta\dot{\Omega}/\dot{\Omega} \sim 10^{-2}$ since its first discovery (Radhakrishnan & Manchester, 1969; Reichley & Downs, 1969). Beside these large glitches, it has also exhibited two extra small glitches. In 1994 it experienced double large glitches ($\Delta\Omega/\Omega = 8.61 \times 10^{-7}$ and $\Delta\Omega/\Omega = 1.99 \times 10^{-7}$) sequentially being separated by 32 days only. Unlike the early Vela glitch observations, which were detected with an uncertainty of weeks in the actual date, recently a continuous monitoring (almost daily since 1985) effort by observers has resulted in uncertainties of less than a day. All of the glitches after the eighth occurred during the observing season and the postglitch relaxation was observed immediately [1]. Postglitch behaviours of the Vela pulsar generally display both exponential relaxation and non-linear response with a constant $\ddot{\Omega}$. While the exponential decays are specified with smaller time scales, in the long run the postglitch relaxation is dominantly characterized by the linear recovery of $\dot{\Omega}$. This is superposed on the short-term exponential decays and persists until the next glitch. The slopes of the long-term linear relaxation, the observed values of $\ddot{\Omega}$, are relatively large for the Vela pulsar. The upper limit of the glitch rise time, which is difficult to be resolved for other sources, is less than 40 s for the Vela pulsar (Dodson, McCulloch & Lewis, 2002).

The vortex creep model (Alpar et al., 1984; Alpar, Cheng & Pines, 1989), attempts to expound the processes causing glitches and postglitch behaviour in terms of the distinct superfluid regions in the inner crust. The theory provides some information on the structure and temperature of neutron star, as well as on the physical properties of the pinned crustal neutron superfluid (Pines & Alpar, 1985). In the superfluid the rotation is carried by quantized vortices which pin to nuclei. The vortex-lattice interaction occurs by thermally activated vortex motion over discrete pinning configuration. Since the crust spins down under the external torque, a lag $\omega = \Omega_s - \Omega_c$ stores between the angular velocities of superfluid and crust. This lag is sustained by the pinning forces acting upon the vortex line until it reaches a maximum value, ω_{cr}, above which the avalanche of vortices takes place in that region (Anderson & Itoh, 1975). In the cylindrical symmetry, this critical lag determined by the maximum pinning force is given by $\omega_{cr} = E_p/rb\rho_s\kappa\xi$, where E_p is the pinning energy, b is the distance between successive pinning sites along the vortex line, κ is quantum of vorticity, ξ is the radius of vortex core, ρ_s is the superfluid density, and r is the distance from the rotation axis. By conservation of angular momentum, this

[1] http://www.jb.man.ac.uk/pulsar/glitches/gTable.html

instantaneous unpinning and outward motion of vortices leads to speeding up of the crust, $\Delta\Omega_c > 0$, called glitch event.

It is an appealing feature for this model that both types of postglitch observation behaviours can be obtained as two regimes of the same physical process. Depending on the pinning energy E_p, the temperature, and the steady state spin-down rate $\dot{\Omega}_\infty$ dictated by the pulsar torque, the postglitch response of a given region can be either linear or non-linear in the glitch induced perturbation. In the linear regime the steady state lag, ω_∞, is much smaller than the critical value, ω_{cr} for unpinning. The response of perturbation to the lag, $\delta\omega = \delta\Omega_s + \Delta\Omega_c$, is linear and gives simple exponential relaxation. In the nonlinear regime, ω_∞ is very close to ω_{cr} and the response to perturbations is highly non-linear. In the long term, after all exponential transients are extracted, the theory can be reduced into three simple equations, including the observable variables associated with glitches (Alpar & Baykal, 2006):

$$I_c \Delta\Omega = (I_A/2 + I_B)\delta\Omega. \tag{3.1}$$

$$\frac{\Delta\dot{\Omega}}{\dot{\Omega}} = \frac{I_A}{I}. \tag{3.2}$$

$$\ddot{\Omega} = \frac{I_A}{I}\frac{\dot{\Omega}_\infty^2}{\delta\Omega}. \tag{3.3}$$

Expressing the angular momentum balance, the first equation gives the glitch magnitude, $\Delta\Omega$. It depends on the change in angular velocity of the superfluid component, $\delta\Omega$, that is related with the number of vortices participating in the glitch event, and the moment of inertia of the regions that vortices pass through, I_A and I_B. Equation (3.2) is about the torques acting on the pulsar. As a glitch occurs, the huge number of vortices move outward as an avalanche. The crust spins up, the lag decreases, and some part of the crustal superfluid decouples from the normal component. Thereby the external torque acts on smaller moment of inertia, which leads to a jump in the spin-down rate. I_B, the moment of inertia of the vortex depletion regions around the creep/vortex vortex trap regions of moment of inertia I_A is not included in this equation. In the traps there is a very high density of vortices around which the local superfluid velocity is too large to permit pinned vortices. Pinning forces are extremely strong within the trap but not in the depletion region. Vortices move very rapidly within this region. This region contributes to

the angular momentum transfer at glitches, while it does not contribute to the spin-down rate (the vortex current) either during or between the time of glitches. Equation (3.3) means that the long term postglitch relaxation is linear in time, $\Delta\dot{\Omega} \propto t$, so that we have a constant second derivative, the slope of the behaviour, for crustal angular velocity. Such behaviour is also seen in most Vela like giant glitches in older pulsars (Yu et al., 2013). Having three equations and three unknowns, I_A, I_B, and $\delta\Omega$, one can solve this set of equations and obtain model parameters.

Alpar et al. (1984) initially analysed the postglitch behaviour of the Vela pulsar for its first four glitches within the vortex creep model. This work used data with major uncertainties in the actual dates of the glitches. After more accurate Vela pulsar glitch observations caught within less than a day, Alpar et al. (1993) focused on the short term response of the pinned crustal superfluid to a glitch as well as exploring the long term angular momentum balance. This work comprehensively evaluates the postglitch relaxation data of the first eight glitches of the Vela pulsar in a self-consistent framework. It describes all eight postglitch data sets in terms of three distinct components which are exponentially relaxed with time scales of 10 hr, 3.2 days and 32 days, followed by a long term recovery of the spindown rate that is linear in time, $\Delta\dot{\Omega} \propto t$. Whereas this long term response describes the nonlinear region through which the sudden motion of vortices takes place at the time of a glitch, the exponentially relaxation terms reflects the linear response of the creep in regions of the crust through which no sudden vortex motion occurred at the time of the glitch.

According to the model, until the whole region A relaxes back to steady state creep, more and more parts of this region reproduces the observed recovery of the change in spin-down rate as a linear function in time:

$$\frac{\Delta\dot{\Omega}(t)}{\dot{\Omega}} = \frac{I_A}{I}\left(1 - \frac{t}{t_g}\right). \tag{3.4}$$

It is assumed that at time t_g, when this recovery complete, the star is back to initial pre-glitch conditions, then the parameter t_g, obtained from the data can be used as an estimate of the time of occurrence of the next glitch. t_g, characterizing the time between glitches, is the time taken by the external torque to refill the maximum glitch induced offset in ω:

$$t_g = \frac{\delta\Omega}{|\dot{\Omega}|_\infty}. \tag{3.5}$$

In the slowing-down neutron stars, glitch conditions will be reached due to enhanced

vortex density in some regions (Chau & Cheng, 1993; Mochizuki & Izuyama, 1995). As the repulsive forces between vortices in these regions are so large, the vortex unpinning happens. The interglitch time interval is interpreted as the time required to re-build up enough vortex density in the unpinning regions. Alpar et al. (1993) estimated the time interval to the next glitch as the time when the nonlinear response, in the form of a constant $\ddot{\Omega}$ has returned to its pre-glitch value. The estimated t_g's were larger than the observed times, t_{obs}, to the glitch for most interglitch intervals. Among the first 8 glitches studied by Alpar et al. (1993), for only the 1971 and 1985 glitches the estimator t_g was shorter than t_{obs}. As a measure of the estimate:

$$M = \sqrt{\frac{1}{8}\sum_{i=1}^{8}\left(\frac{t_{g,i}(\Delta\dot{\Omega}_p) - t_{obs,i}}{t_{obs,i}}\right)^2}, \tag{3.6}$$

we find the rms deviation from the observations as 58.7% for the first 8 glitches.

For the Crab pulsar, assuming that the glitches are pure unpinning events, t_g's are estimated as the order of a few months in disagreement with the observed glitch times (Alpar et al., 1996). This is interpreted as evidence that the glitches in Crab pulsar are not due to vortex unpinning alone. Alpar et al. (1996) proposed that the comparatively small ($\Delta\Omega/\Omega \sim 10^{-8}$) and infrequent ($\sim$ 6 yr interglitch time intervals) events in Crab are triggered by starquakes induced by spin-down (Baym & Pines, 1971; Ruderman, 1976). The crust cracking in conjunction with the vortex creep theory also explains well the abnormal postglitch behaviour (the persistent offset in the spindown rate ($\dot{\Omega}$) in the long run) in the Crab pulsar. According to this, the persistent change in angular acceleration is due to the newly created vortex depletion region by the starquake event at the time of glitch. While this region was sustaining the vortex current before the glitch, there is no longer any contribution to $\dot{\Omega}$ after it. The permanent shift in the spindown rate is given by

$$\frac{\Delta\dot{\Omega}_p}{\dot{\Omega}} = \frac{I_b}{I} \tag{3.7}$$

where $\Delta\dot{\Omega}_p$ is the observed permanent change in $\dot{\Omega}$ and I_b is the moment of inertia of the newly created capacitor regions. The crust quake event is capable to form these regions with the following way: In the crustal lattice quake can release the energy to create lattice deformity. With this new configuration, the newly created pinning centers with a surplus of the local vortex density are generated (Chau & Cheng, 1993). These shifts in $\dot{\Omega}$ are seen to be permanent in the Crab pulsar. In other words, the steady state $\dot{\Omega}$ value for subsequent glitches is permanently reset, to a new value that is less by $\Delta\dot{\Omega}_p$. The next

glitch would then occur roughly when $\dot{\Omega}$ has returned to $\Delta\dot{\Omega}_p$ less than its steady state value $\dot{\Omega}_{n,-}$ before the previous nth glitch:

$$\dot{\Omega}_{n+1,-} = \dot{\Omega}_{n,-} - \Delta\dot{\Omega}_p. \tag{3.8}$$

If such persistent shifts also occur in the Vela pulsar, they would be unresolved in the observed total $\Delta\dot{\Omega}$ in a glitch. However, the post-glitch non-linear recovery at constant $\ddot{\Omega}$ would be completed earlier, as shown in Figure 3.2. In this chapter we re-examine the interglitch time estimator, with the hypothesis that every Vela glitch has a small "persistent shift" as observed in the Crab pulsar. In Section 2 we apply the initial model, without the "persistent shift" scenario to the 1996, 2000, 2004, 2006, and 2010 glitches to obtain the estimate of the times, t_g, between them, and the moment of inertia of the associated non-linear creep regions. In Section 3 we introduce the extended model, incorporating persistent shifts, to derive new estimator t'_g, which are in better agreement with the observed intervals. We discuss our results in Section 4.

3.2 Model Fitting

Alpar et al. (1993) and Chau et al. (1993) examine the post-glitch recovery of the first nine glitches of Vela pulsar. They use the phenomenological vortex creep model in which the post-glitch relaxation is described by the equation:

$$\frac{\Delta\dot{\Omega}_c(t)}{|\dot{\Omega}|_\infty} = -\sum_{i=1}^{2} \frac{I_i}{I}\frac{\Delta\Omega_c(0)}{|\dot{\Omega}|_\infty\tau_i}e^{-t/\tau_i} - \frac{I_3}{I}\frac{\delta\omega(0)}{|\dot{\Omega}|_\infty\tau_3}e^{-t/\tau_3} - \frac{I_A}{I} + \frac{I_A}{It_g}t. \tag{3.9}$$

The first three terms express the short-term exponential relaxation response to a glitch. The remaining two terms are relevant for the long time scale and describe the nonlinear response. Alpar et al. (1993) find that $\tau_1 = 10$ hr, $\tau_2 = 3.2$ days, and $\tau_3 = 33$ days, are essentially unaltered for all Vela glitches. A quick look at the data later interglitch data (1996-2010) shows that by 100 days after each all exponential relaxation components are fully relaxed (Yu et al., 2013). We therefore conservatively choose to use data starting from 100 days after each glitch on our long term fits, with the last two terms in Equation (3.9).

In this work we follow the fitting procedure of the earlier applications to analyze the long term relaxation of 1996, 2000, 2004, 2006, and 2010 glitches of Vela pulsar. We use the Levendberg-Marquardt method to find the best fit values with MPFITFUN

Table 3.1: The inferred and observed parameters for the long term response of the Vela glitches. The entries for the first eight glitches and the ninth glitch are taken from Alpar et al. (1993) and Chau & Cheng (1993) respectively. Errors for the last five parameters are also given in parenthesis.

Year	t_{obs} (days)	t_g (days)	$(I_A/I)_{-3}$	$(I_B/I)_{-3}$
1969	912	1624	7.1	8.4
1971	1491	1375	7.2	8.8
1975	1009	1036	7.2	12.4
1978	1227	1371	6.6	15.2
1981	272	616	6.3	12.2
1982	1067	1485	6.0	8.4
1985	1261	972	6.5	7.9
1988	907	1422	4.7	8.2
1991	1102	1151	7.4	16.2
1996	1190	1086 (3)	6.4 (0.018)	12.9
2000	1634	1719 (2)	6.9 (0.022)	11.5
2004	767	911 (4)	6.7 (0.013)	15.8
2006	1445	1454 (3)	5.2 (0.047)	12.4
2010	1147	985 (8)	5.7 (0.016)	13.5

procedure (Markwardt, 2009)[2]. We only analyze the long term response which reflects the recoupling of the nonlinear creep regions. The relaxation has the behaviour of $\Delta\dot{\Omega}_c \propto t$ at this long time scale. The inferred parameters from the fit (I_A/I, and t_g) and observed times (in days) for 14 glitches of Vela are tabulated in Table 3.1. These results quote the results of Alpar et al. (1993), for the first 8 glitches, of Chau & Cheng (1993) for the 9th glitch, and our results for 5 later glitches. Also included in the Table 3.1 are the associated estimates of I_B/I, the fractional moments of inertia of vortex free regions according to the model (Equation (3.1)) (Alpar et al., 1984). We find that for 10 out of the 14 glitches tabulated, the estimator gives $t_g > t_{obs}$. The root-mean square fractional deviation of the estimator given in Equation (3.11) is now 44.9% for the 14 glitches, compared to 58.7% for the first 8 glitches alone. The fit graphs are shown in Figure 3.1.

3.3 The Modified Interglitch Times of the Vela Pulsar

In the standard vortex creep model (Alpar et al., 1993) it is argued that the influence of crust cracking, which might be significant for young hot pulsars like Crab, becomes unimportant as they evolve to the "Vela-like" pulsars' age: In the young pulsars like Crab the vortex depletion regions (capacitor regions plus vortex traps) are in the formation stage, while this phase is already completed in Vela. It is likely for the glitches of Crab

[2]http://purl.com/net/mpfit

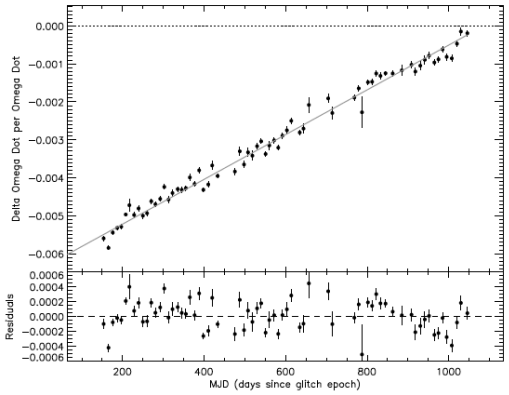

(a) 1996

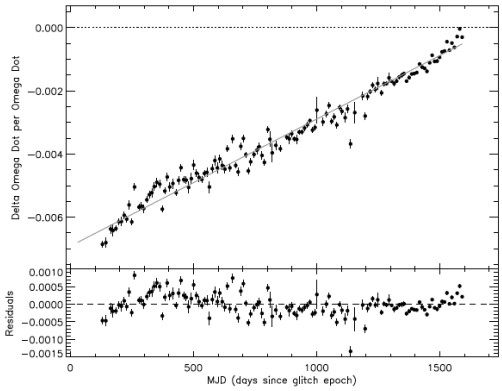

(b) 2000

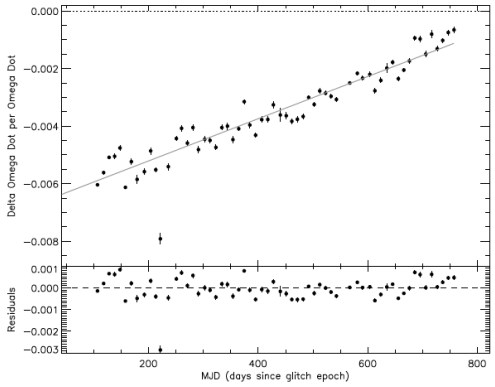

(c) 2004

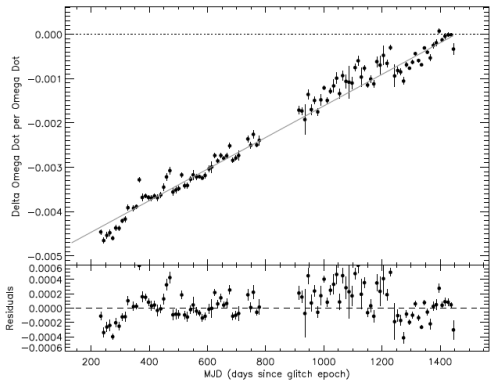

(d) 2006

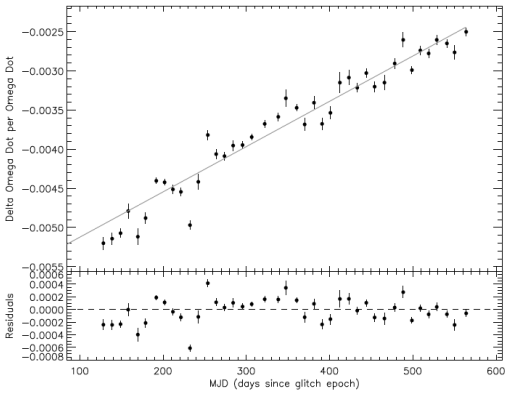

(e) 2010

Figure 3.1: The inferred model fits with the observations of the post-glitch spindown rate of the 1996, 2000, 2004, 2006, 2010 Vela glitches. In the bottom panels the discrepancy between data and model is showed.

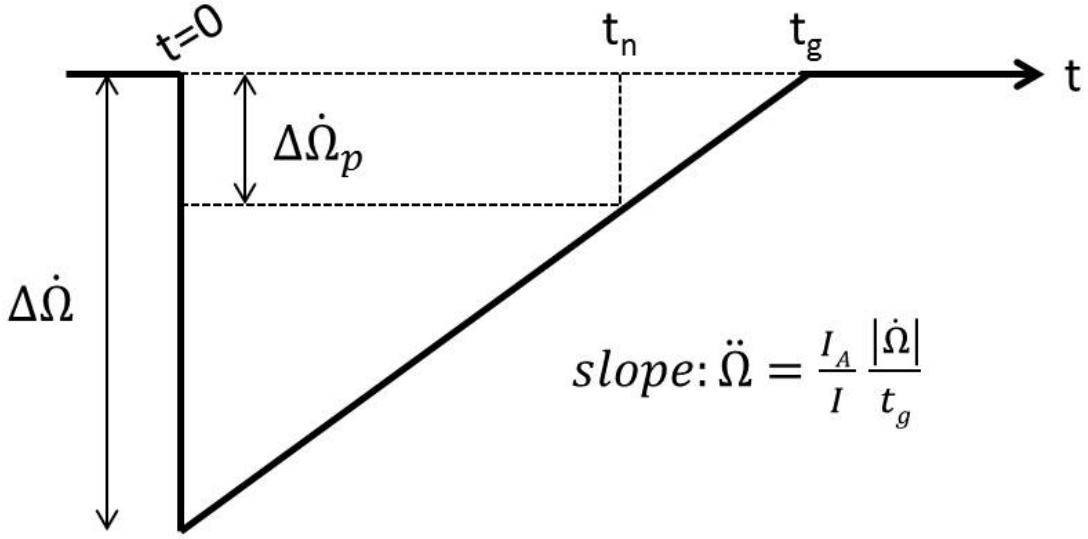

Figure 3.2: The schematic view of the long term behaviour of $\Delta\dot{\Omega}/\dot{\Omega}$

pulsar to be triggered by crust cracking. The permanent step in the spindown rate, $\Delta\dot{\Omega}_p$, which indicates the formation of a new network of vortex depletion regions, has been observed after each glitch in Crab. In this work we propose that Vela is still in the phase of creation of these regions: Exhibiting two distinct extra small glitches, Vela pulsar might also have persistent shifts in spindown rate in all glitches. The part of the $\Delta\dot{\Omega}$ associated with the permanent shift cannot be discerned at the time of the glitch. Being a persistent shift, it will not relax back totally. The part of the step down in $\dot{\Omega}$ that restores with a constant second derivative of Ω will continue the recovery until new steady state conditions, including the persistent shift, are reaches. A schematic view of the long term behaviour of $\dot{\Omega}(t)$ is depicted in Figure 3.2. In this new model, with persistent shift, the triangle has less depth, so the estimated time of the next glitch is a bit shorter. This will make the predicted glitch times closer to the observed values. By using simple geometry, Equations (3.3) and (3.5) to describe the "new" estimated glitch time in terms of the timing parameters of the pulsar, we obtain

$$t'_g = t_g - \frac{|\Delta\dot{\Omega}_p|}{\ddot{\Omega}} = \left(\frac{\Delta\dot{\Omega}}{\dot{\Omega}} - \frac{\Delta\dot{\Omega}_p}{\dot{\Omega}}\right)\frac{\dot{\Omega}}{\ddot{\Omega}} \tag{3.10}$$

where $\Delta\dot{\Omega}$ and $\Delta\dot{\Omega}_p$ is the total and permanent step in spindown rate respectively.

The new calculated time intervals, t'_g, between the glitches are indeed generally closer to the observed values. The value of $\Delta\dot{\Omega}_p/\dot{\Omega}$ is at the order of $\sim 10^{-4}$ for Crab pulsar glitches, it may be different in Vela due to evolutionary reasons. We first assume that all Vela glitches involve the same persistent shift $\Delta\dot{\Omega}_{p,0}$, and choose this to minimize the

Table 3.2: Modified interglitch time estimates with the observation times and fit parameters of Vela glitches with the persistent shift in spindown rate of $\Delta\dot{\Omega}_p/\dot{\Omega} = 1.6 \times 10^{-3}$ rad s^{-2}

Year	t'_g (days)	t_{obs} (days)	$(I_A/I)_{-3}$	$(I_B/I)_{-3}$
1969	1258	912	5.5	12.7
1971	1169	1491	5.6	11.8
1975	936	1009	5.6	14.9
1978	1239	1227	5.0	18.0
1981	460	272	4.7	18.3
1982	1089	1067	4.4	13.5
1985	833	1261	4.9	13.5
1988	938	907	3.1	14.4
1991	1004	1102	5.8	19.6
1996	964	1190	4.8	15.8
2000	1541	1634	5.3	14.0
2004	693	767	5.1	22.6
2006	1207	1445	3.6	16.2
2010	909	1147	4.1	15.7

root-mean square fractional deviation

$$M = \sqrt{\frac{1}{14}\sum_{i=1}^{14}\left(\frac{t'_{g,i}(\Delta\dot{\Omega}_p) - t_{obs,i}}{t_{obs,i}}\right)^2}, \tag{3.11}$$

where t'_g is given by Equation (3.10) for the interglitch fits following glitch i. Fits were performed for full sets of data including N=14 glitches of Vela pulsar. We found $\Delta\dot{\Omega}_{p,0} = 1.6 \times 10^{-3}$ minimizes the rms fractional deviation, M. The rms deviation is then 25.6%, compared to 44.9% for the model without persistent shifts. The observed values of interglitch times and the new estimations for $\Delta\dot{\Omega}_p/\dot{\Omega} = 1.6 \times 10^{-3}$ are listed in Table 3.2. The estimate t'_g is now generally a better estimate of the observed times to the next glitch. For 5 out of the 14 interglitch intervals, the estimated time t'_g is still longer than the observed time to the next glitch $t_{obs,i}$. Table 3.2 also gives the model parameters I_A/I and I_B/I, the fractional moments of inertia of non-linear creep and vortex free regions respectively.

In reality the persistent shift in each glitch is going to be somewhat different. We next calculate the values of $\Delta\dot{\Omega}_p/\dot{\Omega}$ in each glitch that will make $t'_{g,i} = t_{obs,i}$. In Table 3.3 we give these different $\Delta\dot{\Omega}_p/\dot{\Omega}$ values which are found via inserting the observed interglitch times in Equation (3.10), $t'_{g,i} = t_{obs,i}$, together with the parameters from the fits. For the ten glitches this persistent shift is bounded by $10^{-5} < \Delta\dot{\Omega}_p/\dot{\Omega} < 10^{-3}$. We cannot calculate it for the glitches in 1971, 1985, 1996, and 2010 as $t_{obs} > t_g$ for these events. The implied I_A/I and I_B/I values are also given in Table 3.3.

Table 3.3: The persistent steps in spindown rate and associated fit parameters of Vela glitches, needed to give $t'_g = t_{obs}$

Year	$(\Delta\dot{\Omega}_p/\dot{\Omega})_{-3}$	$(I_A/I)_{-3}$	$(I_B/I)_{-3}$
1969	3.11	3.99	19.4
1971	-	-	-
1975	0.18	7.02	12.9
1978	0.61	5.99	17.7
1981	3.2	3.11	33.4
1982	1.7	4.32	13.8
1985	-	-	-
1988	1.6	3.12	15.0
1991	0.32	7.08	16.9
1996	-	-	-
2000	0.34	6.56	12.4
2004	1.1	5.63	19.9
2006	0.032	5.17	12.5
2010	-	-	-

3.4 The Braking Index of the Vela Pulsar

We also re-calculate the true braking index for the Vela pulsar using our results above. Estimating the braking index requires modelling and subtracting all contributions of glitches and interglitch recovery. Lyne et al. (1996) did this by arbitrarily assuming that $\dot{\Omega}$ values 150 days after each glitch are clean of interglitch response and estimated a breaking index $n \cong 1.4$. This approach clearly uses a post-glitch epoch when all short term exponential relaxation components with $\tau_1 = 10$ hr, $\tau_2 = 3.2$ days and $\tau_3 = 32$ days are over, but the interglitch recovery is far from complete. One needs to take account of the constant $\ddot{\Omega}$ response, which extends to the next glitch, the subject of this work. Thus the appropriate epochs when inter-glitch neutron star response is completely recovered should be at t_g, t'_g, or t_{obs} (see Table 3.1 and 3.2), just prior to subsequent glitch.

In this work we obtain the $\dot{\Omega}$ values at these epochs extrapolating from our fits in the model with the Equation (3.3). We then separately produce the very long term (between the years 1969-2013) $\ddot{\Omega}_{PSR}$ values for the vela pulsar by the best linear fit to the $\dot{\Omega}(t'_{g,i})$, $\dot{\Omega}(t_{obs,i})$, and $\dot{\Omega}(t_{g,i})$ data sets given in Figure 3.3. These give the estimates of $\ddot{\Omega}^{t'_g}_{PSR} = (3.62 \pm 0.12) \times 10^{-22}$ rad s^{-3}, $\ddot{\Omega}^{t_{obs}}_{PSR} = (3.83 \pm 0.15) \times 10^{-22}$ rad s^{-3}, $\ddot{\Omega}^{t_g}_{PSR} = (4.14 \pm 0.38) \times 10^{-22}$ rad s^{-3} and that of braking indices $n_{t'_g} = 2.68 \pm 0.09$, $n_{t_{obs}} = 2.81 \pm 0.11$,

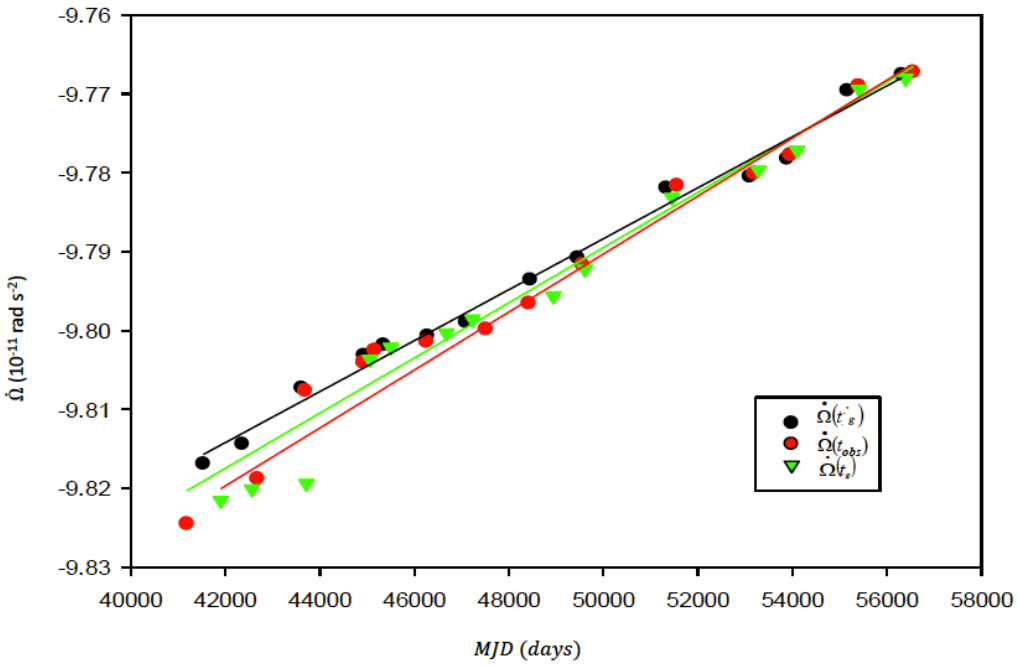

Figure 3.3: The spin-down rate values obtained by the local fits at the epochs t'_g (black points), t_{obs} (red points), and t_g (green points) between the years of 1969 and 2013. The best straight line fits is also showed.

and $n_{t_g} = 2.99 \pm 0.28$ respectively, for Vela pulsar with

$$n = \frac{\overline{\Omega}\ddot{\Omega}_{PSR}}{\left(\dot{\overline{\Omega}}\right)^2}, \tag{3.12}$$

where $\overline{\Omega} = 70.4$ rad s$_{-1}$ and $\dot{\overline{\Omega}} = 9.8 \times 10^{-11}$ rad s^{-2} are the average values over the 44 year data span.

3.5 Conclusions

In this work we have investigated the interglitch time estimates between 14 glitches of Vela pulsar using the vortex creep model. We propose that for each glitch there might be a persistent shift in spindown rate that does not relax back entirely. This step which is observed also in the Crab pulsar, would not be distinguished observationally as a part of the glitch in the spindown rate. We remodel the Vela glitches by introducing a crustquake that induces the new vortex traps. After each event these regions no longer contribute to

spindown and cause a persistent shift in spindown rate. The triangle postglitch behaviour in spindown, which restores with a constant second derivative of Ω, is completed a bit earlier, restoring conditions for a new glitch. Deriving the modified estimator for the time between glitches by using this consideration, we apply this model for 14 Vela glitches spanning 44 years of observation, via the minimizing procedure from which we obtain the common persistent shift ($\Delta\dot{\Omega}_p/\dot{\Omega} = 1.6 \times 10^{-3}$) for all glitches, with the rms deviation of 25.6%, compared to 44.9% for the model without persistent shifts. Hence our new estimates for the interglitch times for Vela agree better with the observed interglitch times. We also close the "optimal conditions" for each glitch by equating the observational interglitch time with t'_g, and obtain different persistent shifts in spindown rate bounded by $3.14 \times 10^{-3} < \Delta\dot{\Omega}_p/\dot{\Omega} < 3.2 \times 10^{-5}$ for each 10 glitch.

We also examine the long term spindown evolution of Vela by re-estimating its braking index. We propose that all glitch contributions are clean of, as the linear recovery with $\ddot{\Omega}$ is fully completed at the time of just before the subsequent glitch which might be t_g, t'_g, or t_{obs}. Unlike the previous work of Lyne et al. (1996) who found $n \approx 1.4$, we obtain the braking index between $2.66 - 3.03$ for Vela.

Chapter 4

MINIMUM GLITCH SIZE OF THE CRAB PULSAR AND THE CRUSTQUAKE AS A TRIGGER MECHANISM

4.1 Introduction

Pulsars, which are thought to be the most exact clocks in the universe (Hobbs et al., 2012), have highly stable spin rates. They are mostly observed to spin-down by electromagnetic emission. Nevertheless they also commonly show timing irregularities in two ways: (i) continuous stochastic deviations from the simple slowdown model ("timing noise"), (ii) abrupt changes in their rotation rates together with increase in the spindown rate ("glitches"). The timing noise is thought be caused by different processes including superfluid turbulence (Melatos & Link, 2014), changes in magnetospheric activity (Shemar & Lyne, 1996; Hobbs, Lyne & Kramer, 2010), and precession (D'Alessandro et al., 1993).

Glitch sizes vary by some orders of magnitude ($10^{-12} < \Delta\Omega/\Omega < 10^{-5}$) (Espinoza et al., 2011) with power law distributions (Melatos, Peralta & Wyithe, 2008). At the lower end, it is hard to resolve the smallest glitches from the "timing noise" events at the lower end of the distributions. A few theoretical models have been produced to explain the large glitches. Models for possible triggers and smallest glitch size have not been detailed and remained untested, because of observational limitations. The smallest observed glitches were barely resolved above the timing noise. Until recently it was not known whether a minimum glitch size existed.

The recent investigation of Espinoza et al. (2014) obtained a level of detection sensitivity that exposed the small events of Crab pulsar which can be identified as glitches. Before this work the smallest glitches, which are thought to be possibly below the detection limits, could not be distinguished from the timing noise. Espinoza et al. (2014) built an "automated glitch detector" to uncover the full distribution of glitch sizes of the Crab pulsar and determined its smallest glitch size as $\Delta\Omega/\Omega \sim 1.7 \times 10^{-9}$, by distinguishing a resolved glitch from timing noise as an abrupt positive step in rotational frequency ($\Delta\Omega > 0$) together with a discrete negative (or null) step in spindown rate. Using X-ray data work by Vivekanand (2016) also reported that Crab might have exhibited a comparable smallest glitch event ($\Delta\Omega/\Omega \sim 1.3 \times 10^{-9}$).

These minimum size glitches in Crab point out that the size of glitch events is distinct from that of timing noise. Glitches are thought to be caused by an abrupt angular momentum transfer from the pinned superfluid component which rotates slightly faster than the solid crust (Anderson & Itoh, 1975). The quantized vortices in the superfluid component interact with the nuclei in the lattice over distinct pinning regions. While the pinned superfluid without outwards vortex motion cannot slow down, the crust slows down by the external torque. A lag between superfluid and crust's angular velocity builds and finally

reaches a critical threshold at which the vortices are abruptly unpinned and move outward freely, leading to speeding up of the crust (the glitch).

A crustquake might also play a significant role as a trigger mechanism for vortex unpinning. Spinning down of the star (Ruderman, 1969; Baym & Pines, 1971), internal electromagnetic strains (Lander et al., 2015), or the vortex-lattice interaction (Ruderman, 1976; Chamel & Carter, 2006; Chau & Cheng, 1993) will cause stresses on the crust. Since it is an elastic medium, the crust has a maximum strain beyond which it can no longer sustain elastic deformations. This leads to seismic activities, i.e. quakes. Some vortices are also affected by the quake leading to unpinning. As these unpinned vortices can induce the others in the radially outer region, the larger glitches can be produced by the outward motion of vortices as an avalanche. This scenario is expected in the "middle aged" (older than 10^4 years), "Vela-like" pulsars in which the development of connections in the network of creep regions have sufficiently ended up. Nevertheless the "Crab-like" pulsars with young age cannot produce larger glitch events due to lacking of these creep regions. The glitch model induced by the crustquake is especially favourable for the glitches of Crab as it can clarify the persistent steps in spindown rate in the long run, as the evidence of the newly-connected network of vortex creep regions (Alpar et al., 1996).

In the spinning down of the star, the fluid core can modify its shape from an oblate spheroid to more spherical form, while the solid crust is strained and has to break to readjust its shape as the strain angle reaches a critical value in the end. By the angular momentum conservation throughout the crustquake, the decrease of the inertial moment produces an increase in the angular velocity:

$$\frac{\Delta\Omega}{\Omega} = \frac{\Delta I}{I} = \frac{\Delta\dot{\Omega}}{\dot{\Omega}}. \tag{4.1}$$

For a pure crustquake (without any associated vortex motion) the first equality reflects the conservation of angular momentum, and the second reflects the constancy of the external torque. The change in the inertial moment of the region affected by the event can be obtained using the first equality and the minimum glitch size. In this work we investigate some crustal properties related with the glitch event by introducing the pure crustquake as a trigger with a few yielding geometries.

4.2 Geometry of the Crustquake and Some Estimates

We propose that the minimum glitch size of Crab is related with a pure crustquake without the amplification due to vortex motion. Modeling the geometry of breaking (or yielding)

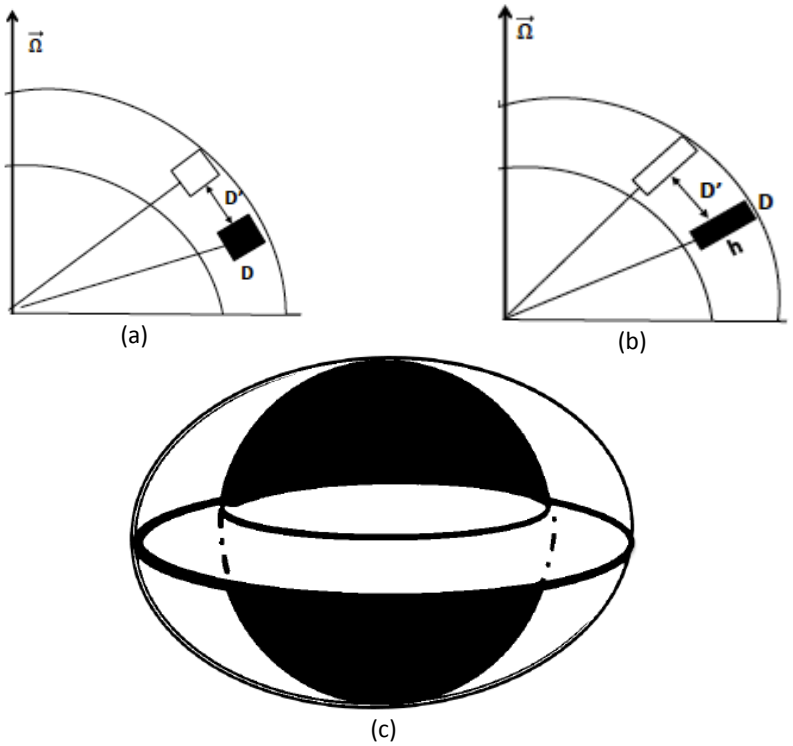

Figure 4.1: Geometries of crust breaking in spindown of the neutron star: (a) a crustal cubic plate, (b) a cylindrical plate moving towards the rotational axis, and (c) a crustal ring, including many plates, moving inward in cylindrical symmetry

in the crust we relate the change in the moment of inertia with the crustal plate(s)'s size, the critical strain angle, and the number of vortices carried by the plate(s) in larger events. We put forth three different geometries that might be associated with this event: (a) a crustal cubic plate (Figure 4.1a), (b) a crustal cylindrical plate which move towards the rotational axis (Figure 4.1b), and (c) a crustal ring which includes many plates and moves inward in the cylindrical symmetry (Figure 4.1c).

Some vortices perturbed by the quake move outward as an avalanche and get unpinned. If these vortices move downstream in the azimuthal direction and induce other vortices to unpin in the slightly outer region, the larger glitches can be created by the amplification of vortex motion. Nevertheless the smallest glitch is caused by only a pure crustquake event during which there is a change in the inertial moment by the crustal plate(s) movement. While the breaking and movement of crust are rigid and irreversible processes, the superfluid component's spindown by vortex flow (creep) can relax back to the pre-glitch states in time.

4.2.1 Size of the Broken Plate(s)

The size of the broken plate can be found by relating it with the change in the moment of inertia of the region where the crustquake takes place. We study this introducing three different geometrical models.

In the first model a cubic crustal plate with the volume of $V = D^3$ moves towards higher latitude by a distance of D' (Figure 4.1a). This crustal movement results in a decrease in the fractional inertial moment of the solid as:

$$\frac{\Delta I}{I} = \frac{m[R^2 - (R - D')^2]}{\frac{2}{5}MR^2} \tag{4.2}$$

where R is the radius, M is the mass of the entire star, m is the mass of the moving plate, and D' is the distance along which the plate flits during the crustquake. m can be related with the volume of plate as $m = \rho_c D^3$ where D is the broken plate size and ρ_c is the mass density of the crustal layer where the quake origins. D and D' are related by a proportionality factor f, $(D' = fD)$, which determines the comparison between the plate size and the distance the plate flits. Using Equation (4.1) with these assumptions and the minimum glitch size, $\Delta\Omega/\Omega = 1.7 \times 10^{-9}$ measured by Espinoza et al. (2014) we find

$$\frac{\Delta\Omega_{min}}{\Omega} = 1.7 \times 10^{-9} \cong 2.5 \times 10^{-10} D_4^4 \left(\frac{M_\odot \rho_{c,13} f}{M R_6}\right) \tag{4.3}$$

Here $\rho_{c,13}$ is the crustal mass density in units of 10^{13} g cm^{-3}, $M_\odot = 2 \times 10^{33}$ g is the solar mass, and R_6 is the neutron star radius in units of 10^6 cm. From this we obtain the size of broken cubic plate as $D \cong 160[(MR_6)/(M_\odot \rho_{c,13} f)]^{1/4}$ meters.

Another geometrical model with the cylindrical plate (Figure 4.1b) only differs by its volume as $V = \pi D^2 h/4$ where D is the diameter and h is the radial thickness of the broken plate. Here the relation between the size of the minimum glitch and the broken plate becomes:

$$\frac{\Delta\Omega_{min}}{\Omega} = 1.7 \times 10^{-9} \cong 1.96 \times 10^{-9} D_4^3 \left(\frac{M_\odot \rho_{c,13} f h_5}{M R_6}\right) \tag{4.4}$$

which gives the plate's diameter as $D \cong 95[(MR_6)/(M_\odot \rho_{c,13} f h_5)]^{1/3}$ meters. In this case since the crustquake takes place locally, we take the radial thickness h_5 (in units of 10^5 cm) as the entire of crust in this geometrical configuration.

The third model is based on the idea that the crust might fail as a whole, not along

the faults, as a result of large strain. This model involves many broken plates of size D within a crustal ring, which is close to the equatorial region, of radius R, with each plate moving a distance $D' = fD$ (Figure 4.1c), so that the volume is taken a $V = 2\pi RDh$. The fractional change in the inertial moment then becomes

$$\frac{\Delta I}{I} \cong \frac{\rho_c(2\pi RDh)(2fDR)}{(2/5)MR^2}. \tag{4.5}$$

Taking the radial thickness, h, as the outer crust (in units of 10^4 cm) due to the fact that the quake occurs in globally geometrical configuration , we estimate the size of the plate as $D \cong 11[M/(M_\odot \rho_{c,13} f h_4)]^{(1/2)}$ meters in this case.

4.2.2 The Critical Strain Angle

We also examine the crustquake model in terms of the critical strain angle, θ_{cr}, at which the yielding takes place in the crustal lattice. We assume that a plate of size D and thickness h is involved in the quake event. Hence the critical strain angle can be simply approximated as

$$\theta_{cr} \sim \frac{D}{h}. \tag{4.6}$$

The estimates of critical strain angle for various geometries using the above estimates of D:

$$\theta_{cr}^{cube} \sim 1.6 \times 10^{-1} \frac{1}{h_5} \left(\frac{(M/M_\odot)R_6}{\rho_{c,13} f} \right)^{1/4}, \tag{4.7}$$

$$\theta_{cr}^{cylinder} \sim 9.5 \times 10^{-2} \frac{1}{h_5} \left(\frac{(M/M_\odot)R_6}{\rho_{c,13} f h_5} \right)^{1/3}, \tag{4.8}$$

$$\theta_{cr}^{ring} \sim 1.1 \times 10^{-1} \frac{1}{h_4} \left(\frac{(M/M_\odot)}{\rho_{c,13} h_4 f} \right)^{1/2}. \tag{4.9}$$

These very rough estimates for θ_{cr} are in agreement with both the results of the molecular dynamical simulations by Horowitz & Kadau (2009) and the estimates we obtain in the next chapter.

4.2.3 Number of Vortices Involved in a Larger Glitch

After being affected by the crustquake and flowing downstream in the azimuthal direction, the vortices can induce other vortices to unpin if they can find the connection of vortex creep network in the outer layer. In older pulsars which exhibit larger glitches connected vortex creep regions are already established. The vortices perturb the other vortices in slightly outer region and stay flowing downstream in that layer, then the induced vortices affect the more outer vortices, and so on. This subsequent vortex avalanche does not occur efficiently in the younger pulsars exhibiting smaller glitches.

Assuming that some vortices are firstly affected or carried by the broken plate, we can also estimate the number of vortices, δN, triggered by the crustquake using the relation of

$$\delta N = A\left(\frac{2\Omega}{\kappa}\right). \tag{4.10}$$

Here A is the area of each plate ($A_{cube} = D^2$, $A_{cylinder} = \pi D^2/4$, $A_{ring} = D^2$), Ω is the angular velocity of star, and κ is the quantum vorticity. These give the estimates for the number of vortices depending on the fracture geometry as:

$$\delta N_{cube} = 4.9 \times 10^{13}\left(\frac{(M/M_\odot)R_6}{\rho_{c,13}f}\right)^{1/2}, \tag{4.11}$$

$$\delta N_{cylinder} = \pi D^2\frac{2\Omega}{\kappa} \sim 3.2 \times 10^{13}\left(\frac{(M/M_\odot)R_6}{\rho_{c,13}fh_5}\right)^{\frac{2}{3}}, \tag{4.12}$$

$$\delta N_{ring} = D^2\frac{2\Omega}{\kappa} \sim 2.3 \times 10^{11}\left(\frac{(M/M_\odot)}{\rho_{c,13}h_4 f}\right). \tag{4.13}$$

In the final case the number of vortices we obtain is 2 order smaller than in the other geometries, since it must include many ($\sim 10^2 - 10^3$) plates that induce more vortices around the ring.

Angular momentum conservation states that (see previous two chapters for more details):

$$\frac{\Delta\Omega}{\Omega} = \left(\frac{I_A}{2I} + \frac{I_B}{I}\right)\frac{\delta\Omega}{\Omega} \tag{4.14}$$

where I_A/I and I_B/I are the fractional moments of inertia of superfluid regions through which the unpinned vortices move rapidly during the glitch, and $\delta\Omega$ is the change in the superfluid rotation rate due to this sudden motion of δN vortices as:

$$\delta N = \frac{2\pi R^2 \delta\Omega}{\kappa}. \tag{4.15}$$

Separate analysis of angular momentum balance in both Vela (Alpar et al., 1993) and Crab (Alpar et al., 1996) pulsars' (also in PSR J1119-6127-see the first chapter) glitches typically yields the same $\delta N \sim 10^{13}$. It is interesting that the δN estimates we obtain here; as the number of vortices giving the avalanche with crust breaking indicated by the minimum glitch is in agreement with this general earlier results. The reason of this very common number in pulsar glitches, irregardless of the pulsar age, the glitch size or the creep regions, has not been well known. Now we propose that this common scale of δN is related with the crustquake as a trigger and some crustal properties including the broken plate size and the geometry of breaking.

4.3 Conclusions

The minimum glitch size of Crab observed by Espinoza et al. (2014), which is exactly uncovered from the timing noise, give the opportunity to take this event into account in terms of the crustquake as a trigger. We propose that the change in the inertial moment is directly related with this minimum glitch size by the pure crustquake model. Introducing some breaking geometries we drive the fractional change of inertial moment due to the plate movement during the crustquake as a function of the broken plate size (Equations (4.2)-(4.5)), D, with some scaling factors, which also determines the estimates of critical strain angle, θ_{cr} and the number of vortices, δN taking part in the larger glitches. These estimates for the Crab pulsar are $D \sim 11 - 160$ m, depending on geometrical assumptions for the plate size, and give the orders of $\theta_{cr} \sim 10^{-1}$ and $\delta N \sim 10^{13}$ which are in a good agreement with the previous works.

The qualitative difference of glitch behaviour of Vela and Crab is due to evolutionary reasons. The moment of inertia involved in a glitch increases with age (Pines & Alpar, 1985). While Vela should already have well connected the creep network so that the large glitches can be created, Crab is still in the stage of creation the creep regions. The common number of vortices taking part in glitch is only about the trigger process.

There are some uncertainties in our estimations: the distance that the broken plate moves during the crustquake, D', and the radial thickness, h, of the plate. D' corresponds

to a change of the inclination angle, $\Delta\alpha$, between the rotation and magnetic axes as the crustquake takes place. This change can be observed in some events (see the first chapter for an attractive example) by a change in the external electromagnetic torque during an extraordinary glitch event. In the pulsars (like PSR 1119-6127), with large magnetic field ($\sim 10^{13}$ G), which produce the crustquake at a location very close to the magnetic axis and/or to the surface of the star, the crustal movement amplified by the elastic response of the field lines can easily affect the magnetospheric activities. This glitch (or crustquake) associated change in the external torque is not observed in Crab, so we cannot determine the shift in the inclination angle, $\Delta\alpha$, and also D'. Instead we associate it with the plate size by a proportional factor as $D' = fD$. Scaling $\Delta\alpha \sim 10^{-4}$ (from the result of the first chapter for PSR 1119-6127) and using the relation of $D' = R\Delta\alpha = fD$ with the our estimates of D we find

$$f \sim 10^{-2} \left(\frac{R_6 \Delta\alpha_{-4}}{D_4} \right). \tag{4.16}$$

Hence we expect that the broken plate moves towards the rotational axis, with a distance smaller than its size, by a proportional factor of $\sim 10^{-2}$, during the crustquake.

Recently the two orders of magnitude smaller glitch size ($\Delta\Omega/\Omega = 2.5 \times 10^{-12}$) has been observed in the millisecond pulsar, J06130200 by McKee et al. (2016). The crustquake model we propose here gives the estimates of its broken plate size as $D_{cube} \cong 38$ m, $D_{cylinder} \cong 13.6$ m, $D_{ring} \cong 0.4$ m for the geometries of cubical plate, cylindrical plate, and ring involving many plates respectively, and also the orders of the critical strain angle and the vortices number as $\theta_{cr} \sim 10^{-2}$ and $\delta N \sim 10^{11} - 10^{12}$. We assume that these different estimates for a millisecond pulsar are due to their very old age. They have experienced many glitches and crustquakes, as well as accreting for a long time so that their crusts may have been distorted many times. Hence their critical strain angle has been reduced (annealed) to maybe $\theta_{cr} \sim 10^{-2}$, reducing the plate size D and the number of unpinned vortices proportionately to give $\delta N \sim 10^{11} - 10^{12}$.

Chapter 5

THE CRITICAL STRAIN ANGLE IN THE NEUTRON STAR CRUST

5.1 Introduction

The neutron star interior is a magnificent cosmic laboratory offering extreme conditions far from the properties of terrestrial matter. The nuclei are arrayed in a (probably bcc) crystalline lattice immersed in a gas of strongly degenerate electrons, which are relativistic at densities above $\rho_{rel} \cong 10^6$ g cm^{-3}. In the inner crust, at densities higher than the neutron drip density, $\rho_{drip} = 4 \times 10^{11}$ g cm^{-3}, matter becomes very neutron rich and some neutrons are in continuum (Bloch) states of the crystal, comprising a BCS superfluid by pinning in the attractive channel of neutron-neutron interactions. Screening of the Coulomb interactions by electrons is negligible, as the Thomas-Fermi screening length is larger than the lattice spacing (Pethick & Ravenhall, 1995). Thus the neutron star crust lattice is expected to be a Coulomb lattice due to the relativistic energies of the degenerate electrons. At the highest densities where the "nuclei" are very close to each other, spherical nuclei are distorted into elongated shapes. Two-dimensional order takes over with spaghetti-like rod "nuclei" containing the bound protons and neutrons. At the highest densities of the inner crust, $\rho \lesssim 10^{14}$ g cm^{-3}, one dimensional order is reached, with alternative slabs containing protons and neutrons, and neutrons only. These transitions to spaghetti-like rods and lasagna-like slabs, called "nuclear pasta" arise where the Coulomb energy is comparable in magnitude with the surface energy of the nuclei (Ravenhall, Pethick & Wilson, 1983; Hashimoto, Seki & Yamada, 1984).

Structure of neutron stars is probed by observations of pulsar glitches. Glitches are sudden changes in rotation frequencies and spindown rates of pulsars. When the first glitches were observed, a "crustquake" scenario was proposed (Baym et al., 1969; Ruderman, 1969). In this early model, the crust occasionally fractures due to stresses induced by spinning down of the star, hence readjusting to a more spherical form which a fluid star would follow while spinning down. In each glitch the reduction in moment of inertia of the crust leads to an increase in the angular velocity by conservation of angular momentum. While the model explains the small glitches like in the Crab pulsar (Wong, Backer & Lyne, 2001) and PSR J0537-6910 (Middleditch et al., 2006b), it is inadequate for larger glitches which occur frequently (2-3 years), as exhibited by the Vela pulsar (Baym & Pines, 1971). Superfluid vortex pinning, unpinning and creep can explain these glitches (Alpar et al., 1993), while crust breaking can play a role as a trigger mechanism (Ruderman, 1976, 1991a,c,b; Akbal et al., 2015)(see also Haskell & Melatos (2015) for a review of glitch models).

A crustquake occurs when the strains in the crust reach a critical strain angle, $\overline{\theta}_{cr}$, characteristic of the lattice. The corresponding maximum stresses are given by $\overline{t}_m = \mu\overline{\theta}_{cr}$,

where the shear modulus, $\mu \approx 10^{30}$ g cm^{-1} s^{-2} for typical equations of state and crusts compositions. The critical strain angle is the parameter that regulates the occurrence of glitches by crust breaking. Elastic properties of the crust are also relevant for other neutron star phenomena, like oscillation modes, gravitational wave emission, magnetar giant flares (Haskell & Melatos, 2015). Smoluchowski (1970) estimated the breaking strain as $10^{-5} < \theta_{cr} < 10^{-3}$ by analogy with terrestrial crystals. However, the analogy with terrestrial matters is not justified, as the very large kinetic energies of the relativistic electrons in the neutron star crust implies that screening is negligible, in contrast to the case in terrestrial crystals. The neutron star crust should be an almost perfect Coulomb lattice. The long range Coulomb coupling should allow plastic deformations, without fracture or formation and motion of dislocations up to much larger strains than observed in terrestrial materials with efficient screening. Alpar & Pines (1985) suggested that $\theta_{cr} \sim 10^{-2} - 10^{-1}$, based on the fine-structure constant as the dimensionless number characterizing Coulomb coupling with the relativistic kinetic energy. Large values of θ_{cr}, corresponding to lack of screening, mean that the crystal is long-range coupled, not able to sustain local dislocations easily. The crystal behaves elastically until critical strains are reached, and then fails collectively. With a molecular dynamics simulation, Horowitz & Kadau (2009) found that $\theta_{cr} = 0.08 - 0.14$ at a particular layer of the neutron star crust, with $\rho = 10^{13}$ g cm^{-3}, $Z = 29.4$ for bcc, fcc and polycrystalline ordering. This work concludes that the crust is very strong and it can support "mountains" so that their gravitational wave radiation might be detectable in large-scale interferometers.

In this paper we hypothesize that the dimensionless value of the ratio of the Coulomb energy to the kinetic energy of the relativistic electrons gives an estimate of the critical strain angle, $\theta_{cr} \sim |E_C|/E_K$, in all densities of the crust including the layers with rod and slab nuclear forms. This is justified as the relativistic electron kinetic energy is the dominant term in the total energy, and much greater than the ions' thermal enegry. The estimation agrees with the numerical calculation of Horowitz & Kadau (2009) at the particular density. We propose generic formulas for estimating the critical strain angle of Coulomb lattices with relativistic electrons, in different dimensionalities in the neutron star crust. In Section 2 we calculate the stored Coulomb potential energy and the kinetic energy of relativistic electrons in one Wigner-Seitz cell for spherical, rod, and slab structures. We estimate the critical strain angle, θ_{cr}, for different densities in the crust in Section 3. We also investigate the weak effect of screening on θ_{cr}. We discuss our results in Section 4.

5.2 The Coulomb Potential Energy and the Kinetic Energy in a Unit Cell

In spherical geometry, the Wigner-Seitz cell has a radius r_c, and the nucleus at the center of the cell has radius R. In cylindrical geometry, the Wigner-Seitz cell is taken to be a cylinder of radius r_c, around a "nucleus" rod of R. In plane (slab) geometry, nuclear slabs of thickness R and slabs containing electrons only, of thickness $(r_c - R)$ alternate.

We calculate the absolute value of the total Coulomb energy, $|E_C| = \int_{cell}(E^2/8\pi)dV$ where the total electric field, E, is found using Gauss' law. We obtain the Coulomb energies for sphere, rod, and slab forms in terms of the cell size, r_c, and the nuclear size, R:

$$|E_C^{sph}| = \frac{3Z^2e^2}{10}\left(\frac{2}{R} - \frac{3}{r_c} + \frac{R^2}{r_c^3}\right), \tag{5.1}$$

$$|E_C^{rod}| = \frac{Z^2e^2}{L}\left(ln\left(\frac{r_c}{R}\right) - \frac{1}{2} + \frac{R^2}{2r_c^2}\right), \tag{5.2}$$

$$|E_C^{slab}| = \frac{\pi Z^2e^2}{6A}\left(r_c - \frac{11R}{8} + \frac{R^2}{2r_c}\right), \tag{5.3}$$

where L is the length of the rod "nucleus" and A is the area of the slab "nucleus".

The total kinetic energy of relativistic electrons in the cell is $E_K = Z(3/4)\hbar c k_F$. Here $k_F = (3\pi^2 Z/V)^{1/3}$ is the fermi wave number where V is the Wigner-Seitz cell volume. The expressions for the kinetic energy for the different configurations are:

$$E_K^{sph} = \frac{3}{4}\left(\frac{9\pi}{4}\right)^{1/3}\hbar c Z^{4/3} r_c^{-1}, \tag{5.4}$$

$$E_K^{rod} \cong \frac{3}{4}\left(3\pi\right)^{1/3}\hbar c Z^{4/3} r_c^{-1}, \tag{5.5}$$

$$E_K^{slab} \cong \frac{3}{4}\left(3\pi^2\right)^{1/3}\hbar c Z^{4/3} r_c^{-1}. \tag{5.6}$$

In the spherical case, Z is the number of protons bound in the nucleus, related to the

number density of electrons through:

$$Z = n_e V_{cell} = n_b \chi V_{cell} \tag{5.7}$$

where n_b is the number density of baryons and χ is the proton (or electron) fraction. In the rod and slab geometries, because the "nuclei" are extended, the cell volumes depend on chosen scales. We chose $L \approx r_c$ for the rod geometry and $A \approx r_c^2$ in the slab geometry, leading to:

$$Z_{rod} \equiv n_e V_{rod} \approx n_e \pi r_c^3, \tag{5.8}$$

$$Z_{slab} \equiv n_e V_{slab} \approx n_e r_c^3. \tag{5.9}$$

5.3 Estimation of the Critical Strain Angle in the Crust

To estimate the critical strain angle θ_{cr} for each nuclear configuration, we take the ratio of the total Coulomb potential energy to the kinetic energy of relativistic electrons. Using Equations (5.1)-(5.6), we obtain:

$$\theta_{cr}^{sph} \cong \frac{2}{5}\left(\frac{4}{9\pi}\right)^{1/3} Z^{2/3}\alpha\left(\frac{2r_c}{R} - 3 + \frac{R^2}{r_c^2}\right), \tag{5.10}$$

$$\theta_{cr}^{rod} \cong \frac{4}{3(3\pi)^{1/3}}\lambda^{2/3} r_c^{2/3}\alpha\left(ln\left(\frac{r_c}{R}\right) - \frac{1}{2} + \frac{R^2}{2r_c^2}\right), \tag{5.11}$$

$$\theta_{cr}^{slab} \cong \frac{2}{9}\left(\frac{\pi}{3}\right)^{1/3} \sigma^{2/3} r_c^{1/3}\alpha\left(r_c - \frac{11R}{8} + \frac{R^2}{2r_c}\right). \tag{5.12}$$

Here $\lambda = Z/r_c$ and $\sigma = Z/r_c^2$ are the charge per unit length for rod geometries and charge per unit area for slab geometries, and α is the fine structure constant.

To obtain the numerical results of the critical strain angle in each density through the crust, we have used the range of R and r_c values obtained by Iida, Watanabe & Sato (2001), who investigated the formation of "pasta" layers by zero temperature stability analysis with respect to perturbations inducing fission and proton clustering, and

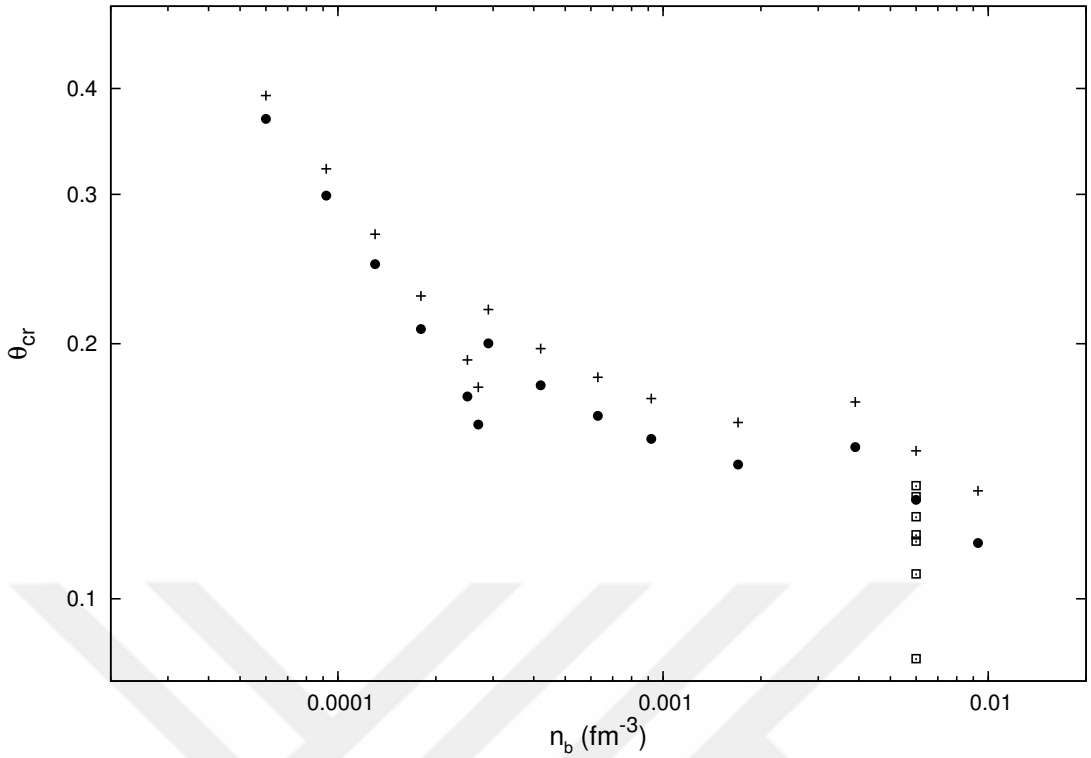

Figure 5.1: Critical strain angle values vs density in the outer crust where the nuclei are spherical Plus signs denote the values of θ_{cr} calculated with the bare Coulomb interaction, bold dots are the values of θ_{cr} calculated with the screened Coulomb interaction. The values of proton number, Z, and the Wigner-Seitz cell size, r_c, are taken from Chamel and Haensel. Square dots at $n_b = 0.006$ fm^{-3} indicate the numerical results of Horowitz & Kadau (2009) for different crystalline structures and strain orientations (see their Figure 1).

Maruyama et al. (2005) who numerically studied the nucleon matter structures at subnuclear densities using density functional theory with relativistic mean fields coupled with the electric field. For the outer part of the crust we take the Z and r_c values presented by Chamel & Haensel (2008). The variation of the critical strain angle values for each layer through the crust is displayed in Figure 5.1 for the outer crust where nuclei are spherical, and in Figure 5.2 and 5.3 for the inner crust, based on values presented by Maruyama et al. (2005), and Iida, Watanabe & Sato (2001). We find $\theta_{cr} \sim 10^{-2} - 10^{-3}$ in the inner crust where the rod and the slab configurations are present.

Horowitz & Kadau (2009) have published the first numerical simulation of θ_{cr} in outer crust layer with density $n_b = 0.006$ fm^{-3}. They find θ_{cr} values ranging from ~ 0.08 for a polycrystalline bcc structure, ~ 0.11 for bcc strain orientations with defects, and $\sim 0.12 - 0.14$ for several strain orientations in bcc and fcc structures. This range is shown in Figure 5.1, along with our results for the outer crust. Our estimation gives $\theta_{cr} = 0.15$ (and $\theta_{cr} = 0.13$ with weak screening) in that layer of the crust. Our estimates for the outer crust are also in agreement with another numerical simulation work by Hoffman & Heyl

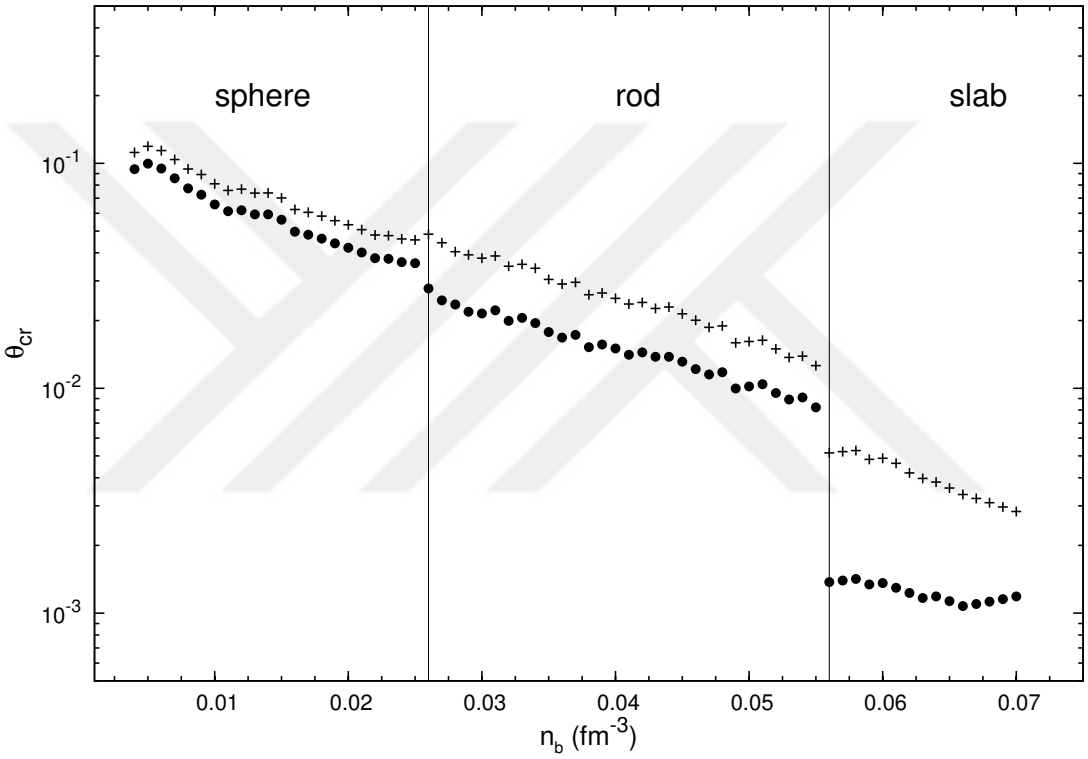

Figure 5.2: Critical strain angle values vs density in the inner crust comprising the 'pasta' layers. Plus signs denote the values of θ_{cr} calculated with the bare Coulomb interaction, bold dots are the values of θ_{cr} calculated with the screened Coulomb interaction. The values of nucleus size, R, and the Wigner-Seitz cell size, r_c, are taken from Maruyama et al. (2005).

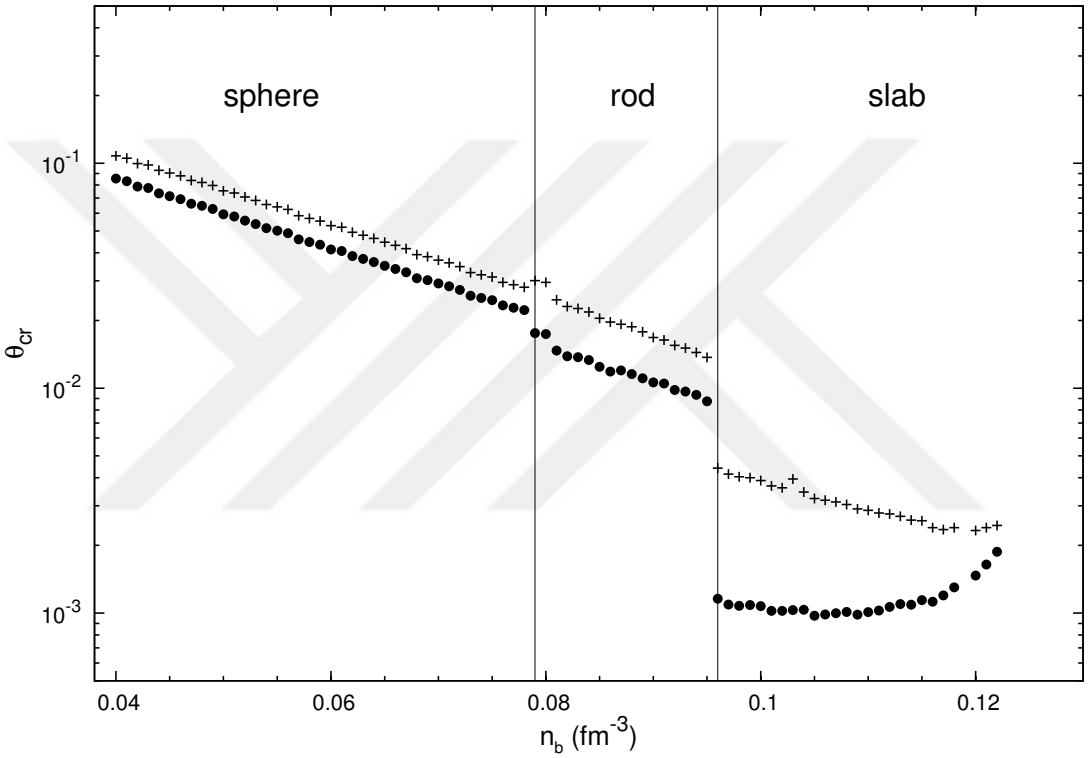

Figure 5.3: Critical strain angle values vs density in the inner crust comprising the 'pasta' layers. Plus signs denote the values of θ_{cr} calculated with the bare Coulomb interaction, bold dots are the values of θ_{cr} calculated with the screened Coulomb interaction. The values of nucleus size, R, and the Wigner-Seitz cell size, r_c, are taken from Iida, Watanabe & Sato (2001).

(2012).

We note that the slabs in the 1-D geometry can easily slide against each other along the plane surfaces between them, behaving like a "liquid crystal" (Ravenhall, Bennett & Pethick, 1972). The 1-D lattice cannot sustain strains and stresses, unless the slab surfaces have rigid long-lived perturbations that break the 1-D symmetry. The critical strain angle, θ_{cr}, may not have a meaning in a 1-D geometry, and the estimate of $|E_C|/E_K$ does not have a bearing on the rigidity of the 1-D lattice.

5.3.1 The Screening Effect

We include the screening effect using the Thomas-Fermi method. In a spherical geometry, the electrostatic potential ϕ is given by the Thomas-Fermi equation:

$$\left(\nabla^2 - \kappa^2\right)\phi(r) = -4\pi n Z e \tag{5.13}$$

where $\kappa = (4\alpha/\pi)^{1/2}(3\pi^2 n_e)^{1/3}$ is the inverse of the screening length of the relativistic electrons, and n is the proton number density. This yields the Yukawa potential, $\phi_r = (Z^2e^2/r)exp(-\kappa r)$ for a point-like nucleus. We apply the Thomas-Fermi model to a finite spherical nucleus with radius R and also rod and slab geometries.

Solving this differential equation in spherical coordinates, polar coordinates and cartesian coordinates for the spherical, rod, and slab crystal structures respectively and using the relation $\overrightarrow{E} = \overrightarrow{\nabla}\phi$, we obtain the screened electric fields in one cell. By using $|E_C| = \int_{cell}(E^2/8\pi)dV$ and $\theta_{cr} \sim |E_C|/E_K$ with screened electric fields we find the estimate of the critical strain angle for the spherical geometry:

$$\theta_{cr}^{sph,scr} \cong \frac{4}{3}\left(\frac{4}{9\pi}\right)^{1/3} Z^{2/3}\alpha r_c \left[\frac{1}{Z^2e^2}\left(E_C^{sph,in} + E_C^{sph,out}\right)\right] \tag{5.14}$$

where $E_C^{sph,in}$ and $E_C^{sph,out}$ are the Coulomb potential energies of the spherical nucleus and the rest of the Wigner-Seitz cell respectively, which are expressed as:

$$E_C^{sph,in} = \frac{Z^2e^2}{10}\left(\frac{1}{R} + \frac{R^5}{r_c^6} - \frac{2R^2}{r_c^3}\right) \tag{5.15}$$

$$E_C^{sph,out} = \frac{9Z^2e^2}{2R^6\kappa^4}\left(Rcosh(\kappa R) - \frac{1}{\kappa}sinh(\kappa R)\right)^2 \Bigg\{\left[\left(\frac{\kappa}{2}+\frac{1}{R}\right)exp(-2\kappa R) - \left(\frac{\kappa}{2}+\frac{1}{r_c}\right)exp(-2\kappa r_c)\right] + \frac{exp(-2\kappa r_c)}{3r_c^2}\left(\kappa+\frac{1}{r_c}\right)^2\left(r_c^3 - R^3\right) - \frac{2exp(-\kappa r_c)}{r_c}\left(\kappa+\frac{1}{r_c}\right)\left[\left(R+\frac{2}{\kappa}\right)exp(-\kappa R) - \left(r_c+\frac{2}{\kappa}\right)exp(-\kappa r_c)\right]\Bigg\}. \tag{5.16}$$

For the rod geometry:

$$\theta_{cr}^{rod,scr} \cong \frac{4}{3}\left(\frac{1}{3\pi}\right)^{1/3}\alpha\lambda^{2/3}r_c^{2/3}\left[\frac{r_c}{Z^2e^2}\left(E_{in}+E_{out}\right)\right]. \tag{5.17}$$

where $E_C^{rod,in}$ and $E_C^{rod,out}$ are the Coulomb potential energies of the cylindrical nucleus and the rest of the Wigner-Seitz cell respectively, which are expressed as:

$$E_C^{rod,in} = \frac{Z^2e^2}{4r_c}\left(1 - \frac{2R^2}{r_c^2} + \frac{R^4}{r_c^4}\right) \tag{5.18}$$

$$E_C^{rod,out} = \frac{Z^2e^2}{r_c}\Bigg\{\left[ln\left(\frac{r_c}{R}\right) + \frac{exp(-2\kappa r_c)}{2r_c^2}\left(r_c^2 - R^2\right)\right] - \left[\frac{2exp(-\kappa r_c)}{\kappa r_c}\left(exp(-\kappa R) - exp(-\kappa r_c)\right)\right]\Bigg\}. \tag{5.19}$$

For the slab form:

$$\theta_{cr}^{slab,scr} \cong \frac{4}{3}\left(\frac{1}{3\pi^2}\right)^{1/3}\sigma^{2/3}r_c^{1/3}\alpha\left[\frac{r_c^2}{Z^2e^2}\left(E_C^{slab,in}+E_C^{slab,out}\right)\right] \tag{5.20}$$

where $E_C^{slab,in}$ and $E_C^{slab,out}$ are the Coulomb potential energies of inner and outer regions of the slab nucleus respectively and expressed as:

$$E_C^{slab,in} = \frac{\pi Z^2e^2}{48}\frac{R}{r_c^2}\left(1 - \frac{2R}{r_c} + \frac{R^2}{r_c^2}\right) \tag{5.21}$$

$$E_C^{slab,in} = \frac{2\pi Z^2e^2}{r_c^2R^2\kappa^2}sinh^2\left(\frac{\kappa R}{2}\right)\Bigg[\frac{1}{2\kappa}\left(exp(-\kappa R) - exp(-2\kappa r_c)\right) - \frac{2}{\kappa}exp(-\kappa r_c)\left(exp(-\kappa R/2) - exp(-\kappa r_c)\right) + exp(-2\kappa r_c)\left(r_c - \frac{R}{2}\right)\Bigg]. \tag{5.22}$$

Here our assumption is that the "naked" Coulomb interaction can be taken inside the "nuclear" regions for all configurations since $\kappa r \ll 1$ here. We also take into account the charge neutrality in the cell and continuity of the potential at the nuclear boundary R. Figure 5.1, 5.2, and 5.3 also contain the numerical results of the screening impact to the critical strain angle which does not differ appreciably as expected.

5.4 Discussion and Conclusions

We have estimated the critical strain angle, θ_{cr} in the neutron star crust by associating it with the ratio between the Coulomb potential energy and the kinetic energy of the relativistic electrons in a cell: $\theta_{cr} \sim |E_C|/E_K$. Our estimates cover crust layers at densities between 6×10^{-4} fm$^{-3} < n_B < 0.12$ fm^{-3}, and crystal structures with spherical nuclei (3-D), as well as rod (2-D) and slab (1-D) phases. The estimate scales with the fine structure constant and the charge or charge density on the "nuclei", and on the microscopic length scales of the "nuclei" and the lattice, R and r_c, in different fashions depending on the geometry. Obtaining estimates of θ_{cr} for all layers of the crust, we conclude that the crust is stronger in the outer region. Our results are compatible with the θ_{cr} value computed with the molecular dynamics simulation, to date, performed by Horowitz & Kadau (2009). This supports our suggestion that θ_{cr} can be estimated easily throughout the different density layers and crystalline phases of the neutron star crust, based on the hypothesis that $\theta_{cr} \sim |E_C|/E_K$. The simplicity is based on the extreme Coulomb crystal situation in the neutron star crust. In actual terrestrial crystals, the effect of screening, defects and anisotropies will dominate in determining the elastic properties, precluding such simple estimations.

We find that θ_{cr} decreases with increasing density and is lower in the 2-D and 1-D phases at densities where the phase transition occurs. The crust is more inclined to break in the inner regions. The crust is strained in consequence of the spinning down of the star or internal electromagnetic effects. The evolution of crustal deformations and occurrence of crustquakes depends on the values of the critical strain angles throughout the crust. We expect that the crust breaking will originate at the innermost regions and may propagate toward the surface. This is consistent with the idea that crustquakes may be triggering glitches amplified by vortex unpinning, allowing unpinned vortices to avalanche outwards through the entire crust.

The 1-D geometry may actually have no role in crust breaking, as slabs in 1-D cannot sustain shear strains and stresses. So the inner crust layers with 2-D rod nuclei is the likely initial site of crust breaking events.

Our finding, in accordance with the results of Horowitz & Kadau (2009), that the outer crust has $\theta_{cr} \sim 10^{-1}$ is encouraging for prospects of detecting gravitational radiation due to "mountains" in neutron stars. We find $\theta_{cr} \cong 0.39$ at the lowest density we have investigated, $n_b = 6 \times 10^{-5}$ fm^{-3} ($\rho \cong 10^{11}$ g cm^{-3}). To extrapolate to lower densities we write Equation (5.10) in the form

$$\theta_{cr} \cong \frac{4\alpha Z}{5R(3\pi^2 n_b \chi)^{1/3}}. \tag{5.23}$$

Employing the values listed in Chamel & Haensel (2008), taking $R = 7$ fm, and $\chi = 0.5$ in the outermost crust we obtain $\theta_{cr} \cong 1.7$ at $\rho = 2.71 \times 10^8$ g cm^{-3}, and $\theta_{cr} \cong 5.2$ at $\rho = 8.02 \times 10^6$ g cm^{-3}, where electrons are still relativistic. In view of the limited range of Z dictated by nuclear physics and weak dependence on the density, we find rather large estimates for $\theta_{cr} \sim |E_C|/E_K$ in the outer crust at 10^6 g cm$^{-3} < \rho < 10^8$ g cm^{-3}. It should be noted that these very large estimates of θ_{cr} do not have a meaning in the assumed linear regime of the stress-strain relation. Our approach is not consistent at these densities. In any case, the thickness δr of the outer crust between 10^6 g cm$^{-3} < \rho < 10^8$ g cm^{-3} is estimated as only a few meters, so these upper layers of the crust will not be important. We shall use our estimate upto $\theta_{cr} \cong 0.39$ at the density of $n_b = 6 \times 10^{-5}$ fm^{-3}.

The strain amplitude of gravitational wave that is the direct impact of a deformation (i.e. mountain) on the neutron star surface is given by (Ushomirsky, Cutler & Bildsten, 2000):

$$h = \frac{16}{5}\left(\frac{\pi}{3}\right)^{1/3} \frac{GQ_{22}\Omega^2}{dc^4}. \tag{5.24}$$

Here d is the distance to the neutron star, Ω is the angular frequency, and Q_{22} is the quadrupole moment which is the outcome of the asymmetric orientation of a deformation (mountain) with respect to the rotational axis and directly related with the critical strain angle (Ushomirsky, Cutler & Bildsten, 2000). The maximum quadrupole moment is given by

$$Q_{22} = \gamma \int \frac{\theta_{cr}(r)\mu(r)r^5 dr}{GM(r)} \tag{5.25}$$

where μ is the shear modulus, $M(r)$ is the enclosed mass within radius r, G is the gravitational constant, and γ is a numerical factor depending weakly on the mass and radius of star, and the crust-core boundary location. We will take into account only the limits

of the crust with spherical nuclear clusters, as the rod and slab layers sustain much lower strains. The molecular dynamics simulations of Hoffman & Heyl (2012) for spherical nuclei give a critical strain angle, θ_{cr} that is independent of position in the crust, while our estimates depend on the properties of the lattice at each layer of the crust. The shear modulus $\mu = (Z^2e^2/a^4)\mu_*$, where μ_* is the dimensionless shear modulus, is also found to be a constant throughout the crust (Hoffman & Heyl, 2012). Taking our variable $\theta_{cr}(r)$ and $\mu = [Z^2(r)/a^4(r)]e^2\mu_*$, which are dependent on the position in the crust we find

$$Q_{22} = \frac{\gamma\mu_* R^5 e^2}{GM} \frac{\theta_{cr}(r_{out}) Z^2(r_{out})}{a^4(r_{out})} \int_{r_{in}}^{r_{out}} f(r) dr. \tag{5.26}$$

Here r_{in} and r_{out} are the boundaries of the crust layers with the spherical nuclei. Also we have made the approximation $M(r) = M$ and $r = R$ throughout the crust, where $M(r)$ is the mass enclosed within radius r and M and R the mass and radius of the neutron star respectively. The function $f(r)$ is defined as

$$f(r) = \left(\frac{a^4(r_{out})}{\theta_{cr}(r_{out}) Z^2(r_{out})} \right) \left(\frac{\theta_{cr}(r) Z^2(r)}{a^4(r)} \right). \tag{5.27}$$

We obtain:

$$Q_{22} \cong \frac{\gamma\mu_* R^5 e^2 \Delta R}{GM} \int_0^1 f(x) dx \tag{5.28}$$

where $x = (r - r_{in})/\Delta R)$ and $\Delta R = r_{out} - r_{in}$ is the thickness of the crust. This gives $Q_{22} \cong 2.8 \times 10^{39}$ g cm^2 and $h = 6.7 \times 10^{-10}(\Omega^2/d)$ by Equation (5.24).

For the millisecond pulsars due to their old age and accretion history, the crust, which have been broken and distorted many times, must be weaker than the younger pulsars', so $\theta_{cr} \cong 10^{-2}$ is likely. Assuming that the maximum θ_{cr} value can still be relevant to the current triaxiality, the expected gravitational wave amplitude h can only be applied for the fast spinning nearby young pulsars and millisecond pulsars.

Summary

This thesis involves the studies of characteristics of the neutron star crust related to the rotational dynamics of isolated neutron stars, especially their remarkable events known as glitches. Rotating neutron stars are observed as spinning down very slowly and in steady state over time by loosing rotational energy. However they (mostly young pulsars) sometimes spin up abruptly. These events, referred as rotational glitches, are thought to be due to the angular momentum transfer from the neutron superfluid component in the inner crust to all other components which are strongly coupled each other by electromagnetic interactions. The superfluid neutrons cannot slow down and rotate with a different rate, since the vortices in superfluid can pin to the crustal lattice, creating the traps with high vortex density. Hence some parts of the superfluid components in the neutron star crust can rotate faster than the observed rotational frequency. As the vortices are released from these pinning sites as an avalanche to arrange all components to co-rotate, spinning up of the crust is observed as the rotational glitches. The glitch size is related with the number of vortices and the inertial moment of superfluid region involved in this event. Glitches are likely triggered by crust breaking, for which the critical strain angle, θ_{cr}, is an important quantity.

Glitches generally are not correlated with the changes in the electromagnetic signature of pulsars. However, in 2007, the glitch of PSR J1119-6127, coexisting with the change in emission pulse profile by displaying RRAT behaviour and switching on intermittent pulses, is firstly observed. This glitch is also unconventional with its anomalous sign signatures: The pulsar is observed rotating with a smaller rotational rate compared with the pre-glitch value, $\Delta\Omega(t) < 0$. It also slows down with a lower rate in the long run, $\Delta\dot{\Omega} > 0$. Chapter 2 presents the investigation of this abnormal glitch behaviour by extending the vortex creep model with the starquake scenario. We propose that with a quake the crustal broken plate moving towards the rotational poles of the star induces inward vortex motion, causing such abnormal glitch signature, and also decreases the perpendicular component of the magnetic field, giving rise to anomalous emission properties. Our model involves the contribution of vortex creep response to glitch, associated with inward and outward vortex motion, as well as that of permanent change in the external torque. With the model fitting we obtain some structural properties of the crust, such as the total moment of inertia of the superfluid creep regions, the size of broken plate, the number of vortices participating in this glitch.

The vortex creep model describes well the post-glitch behaviour in terms of different superfluid regions in the inner crust. It explains the large and frequent glitches of Vela and other pulsars in terms of some structural parameters, as well as the anomalous post-

glitch behaviour of Crab in which there is a persistent offset in $\dot{\Omega}$. However it has the difficulties to estimate the times between glitches in the Vela pulsar. In Chapter 3 we derive a modified estimator of interglitch times, proposing that Vela is still in the stage of creating vortex depletion regions as a result of the crustquake at the time of glitch. These regions, no longer contributing to $\dot{\Omega}$, cause the persistent shifts in spindown rate, like in Crab, which might not be resolved observationally in the part of the large glitch size of Vela. The new estimates for the interglitch times are in better agreement with the observed values. We also estimate the true braking index of Vela, considering that all glitch contributions must be clean of at these epochs, and find it as between $n = 2.66 - 3.03$.

The minimum glitch size of Crab uncovered from the timing noise gives the clue to describe this event in terms of trigger mechanism. In Chapter 4 we model the crustquake as a trigger and obtain the estimates for some crustal quantities by introducing three breaking geometries: (i) a crustal cubic plate, (ii) a cylindrical plate moving towards the rotational axis, and (iii) a crustal ring with many plates moving inward in cylindrical symmetry. We find that the plate size is bounded by 160 m $< D < 11$ m, while the critical strain angle at which a crustquake occurs and the number of vortices in larger glitches are at the order of $\theta_{cr} \sim 10^{-1}$ and $\delta N \sim 10^{13}$ respectively. This gives an understanding of why δN is always found to be of order 10^{13} in model fits to glitches which differ in magnitude by 10^3.

The most important parameter in the crustquake event is the critical strain angle, θ_{cr}. In Chapter 5 we estimate θ_{cr} for the neutron star by taking into account the microphysical structures of the crust in various densities. We associate θ_{cr} with the ratio between the Coulomb potential energy and the kinetic energy of the relativistic electrons in a Wigner-Seitz cell and find that it generally scales with the fine structure constant, the charge Z, and some microscopic length scales. We find that $\theta_{cr} \sim 10^{-1}$ in the outer crust, in agreement with the previous numerical results, where the nuclear shape is spherical, while it reduces to $\sim 10^{-3} - 10^{-2}$ in the inner crust with the rod and slab nuclear configurations. Hence we conclude that the crust is stronger in the outer crust. Our results give an estimate for maximum gravitational wave signatures expected from pulsars.

Bibliography

Akbal O., Gügercinoğlu E., Şaşmaz Muş S., Alpar M. A., 2015, mnras, 449, 933

Alpar M. A., 1977, apj, 213, 527

Alpar M. A., Baykal A., 2006, mnras, 372, 489

Alpar M. A., Chau H. F., Cheng K. S., Pines D., 1993, apj, 409, 345

Alpar M. A., Chau H. F., Cheng K. S., Pines D., 1996, apj, 459, 706

Alpar M. A., Cheng K. S., Pines D., 1989, apj, 346, 823

Alpar M. A., Langer S. A., Sauls J. A., 1984, apj, 282, 533

Alpar M. A., Pines D., 1985, nat, 314, 334

Alpar M. A., Pines D., Anderson P. W., Shaham J., 1984, apj, 276, 325

Anderson P. W., Itoh N., 1975, nat, 256, 25

Andersson N., Glampedakis K., Ho W. C. G., Espinoza C. M., 2012, Physical Review Letters, 109, 241103

Andersson N., Sidery T., Comer G. L., 2006, mnras, 368, 162

Antoniadis J. et al., 2013, Science, 340, 448

Antonopoulou D., Weltevrede P., Espinoza C. M., Watts A. L., Johnston S., Shannon R. M., Kerr M., 2015, mnras, 447, 3924

Archibald R. F. et al., 2016, apjl, 819, L16

Archibald R. F. et al., 2013, nat, 497, 591

Avogadro P., Barranco F., Broglia R. A., Vigezzi E., 2008, Nuclear Physics A, 811, 378

Bardeen J., Cooper L. N., Schrieffer J. R., 1957, Physical Review, 108, 1175

Baym G., Pethick C., Pines D., Ruderman M., 1969, nature, 224, 872

Baym G., Pines D., 1971, Annals of Physics, 66, 816

Beloborodov A. M., 2009, apj, 703, 1044

Blandford R. D., Romani R. W., 1988, mnras, 234, 57P

Bohr A., Mottelson B. R., Pines D., 1958, Physical Review, 110, 936

Camilo F., Kaspi V. M., Lyne A. G., Manchester R. N., Bell J. F., D'Amico N., McKay N. P. F., Crawford F., 2000, apj, 541, 367

Chamel N., 2013, Physical Review Letters, 110, 011101

Chamel N., Carter B., 2006, mnras, 368, 796

Chamel N., Haensel P., 2008, Living Reviews in Relativity, 11

Chau H. F., Cheng K. S., 1993, prb, 47, 2707

Chau H. F., McCulloch P. M., Nandkumar R., Pines D., 1993, apjl, 413, L113

Chen W. C., Li X. D., 2006, aap, 450, L1

Cheng K. S., Alpar M. A., Pines D., Shaham J., 1989, in NATO Advanced Science Institutes (ASI) Series C, Vol. 262, NATO Advanced Science Institutes (ASI) Series C, Ögelman H., van den Heuvel E. P. J., eds., p. 503

Cheng K. S., Pines D., Alpar M. A., Shaham J., 1988, apj, 330, 835

Cooper L. N., Mills R. L., Sessler A. M., 1959, Physical Review, 114, 1377

Cordes J. M., Downs G. S., 1985, apjs, 59, 343

D'Alessandro F., 1996, apss, 246, 73

D'Alessandro F., McCulloch P. M., King E. A., Hamilton P. A., McConnell D., 1993, mnras, 261, 883

Datta B., Alpar M. A., 1993, aap, 275, 210

Demorest P. B., Pennucci T., Ransom S. M., Roberts M. S. E., Hessels J. W. T., 2010, nat, 467, 1081

Dib R., Kaspi V. M., Gavriil F. P., 2009, apj, 702, 614

Dodson R., Lewis D., McCulloch P., 2007, apss, 308, 585

Dodson R. G., McCulloch P. M., Lewis D. R., 2002, apjl, 564, L85

Eastlund B. J., 1968, nat, 220, 1293

Espinoza C. M., Antonopoulou D., Stappers B. W., Watts A., Lyne A. G., 2014, mnras, 440, 2755

Espinoza C. M., Lyne A. G., Stappers B. W., Kramer M., 2011, mnras, 414, 1679

Franco L. M., Link B., Epstein R. I., 2000, apj, 543, 987

Ginzburg V. L., Zaitsev V. V., 1969, nat, 222, 230

Gold T., 1968, nat, 218, 731

Goldreich P., Julian W. H., 1969, apj, 157, 869

Gügercinoğlu E., Alpar M. A., 2014, apjl, 788, L11

Gürkan M. A., Baykal A., Alpar M. A., Ögelman H. B., Strohmayer T., 2000, aap, 356, 1136

Hashimoto M., Seki H., Yamada M., 1984, Progress of Theoretical Physics, 71, 320

Haskell B., Antonopoulou D., 2014, mnras, 438, L16

Haskell B., Melatos A., 2015, International Journal of Modern Physics D, 24, 1530008

Haskell B., Pizzochero P. M., Sidery T., 2012, mnras, 420, 658

Hewish A., Bell S. J., Pilkington J. D. H., Scott P. F., Collins R. A., 1968, nat, 217, 709

Ho W. C. G., Andersson N., 2012, Nature Physics, 8, 787

Hobbs G. et al., 2012, mnras, 427, 2780

Hobbs G., Lyne A., Kramer M., 2006, Chinese Journal of Astronomy and Astrophysics Supplement, 6, 169

Hobbs G., Lyne A. G., Kramer M., 2010, mnras, 402, 1027

Hoffman K., Heyl J., 2012, mnras, 426, 2404

Horowitz C. J., Kadau K., 2009, Physical Review Letters, 102, 191102

Iida K., Watanabe G., Sato K., 2001, Progress of Theoretical Physics, 106, 551

Kaspi V. M., Gavriil F. P., 2003, apjl, 596, L71

Kaspi V. M., Gavriil F. P., Woods P. M., Jensen J. B., Roberts M. S. E., Chakrabarty D., 2003, apjl, 588, L93

Keane E. F., McLaughlin M. A., 2011, Bulletin of the Astronomical Society of India, 39, 333

Keith M. J., Shannon R. M., Johnston S., 2013, mnras, 432, 3080

Kramer M., Lyne A. G., O'Brien J. T., Jordan C. A., Lorimer D. R., 2006, Science, 312, 549

Lander S. K., Andersson N., Antonopoulou D., Watts A. L., 2015, mnras, 449, 2047

Large M. I., Vaughan A. E., Mills B. Y., 1968, nat, 220, 340

Link B., 2014, apj, 789, 141

Link B., Epstein R. I., Baym G., 1992, apjl, 390, L21

Link B., Epstein R. I., Lattimer J. M., 1999, Physical Review Letters, 83, 3362

Link B. K., Epstein R. I., 1991, apj, 373, 592

Livingstone M. A., Kaspi V. M., Gavriil F. P., 2010, apj, 710, 1710

Livingstone M. A., Kaspi V. M., Gavriil F. P., Manchester R. N., Gotthelf E. V. G., Kuiper L., 2007, apss, 308, 317

Lyne A., Hobbs G., Kramer M., Stairs I., Stappers B., 2010, Science, 329, 408

Lyne A. G., McLaughlin M. A., Keane E. F., Kramer M., Espinoza C. M., Stappers B. W., Palliyaguru N. T., Miller J., 2009, mnras, 400, 1439

Lyne A. G., Pritchard R. S., Graham-Smith F., 1993, mnras, 265, 1003

Lyne A. G., Pritchard R. S., Graham-Smith F., Camilo F., 1996, nat, 381, 497

Lyutikov M., 2013, ArXiv e-prints

Manchester R. N., Hobbs G., 2011, apjl, 736, L31

Manchester R. N., Hobbs G. B., Teoh A., Hobbs M., 2005, VizieR Online Data Catalog, 7245

Markwardt C. B., 2009, in Astronomical Society of the Pacific Conference Series, Vol. 411, Astronomical Data Analysis Software and Systems XVIII, Bohlender D. A., Durand D., Dowler P., eds., p. 251

Maruyama T., Tatsumi T., Voskresensky D. N., Tanigawa T., Chiba S., 2005, prc, 72, 015802

McKee J. W. et al., 2016, ArXiv e-prints

Melatos A., Link B., 2014, mnras, 437, 21

Melatos A., Peralta C., Wyithe J. S. B., 2008, apj, 672, 1103

Melatos A., Warszawski L., 2009, apj, 700, 1524

Middleditch J., Marshall F. E., Wang Q. D., Gotthelf E. V., Zhang W., 2006a, apj, 652, 1531

Middleditch J., Marshall F. E., Wang Q. D., Gotthelf E. V., Zhang W., 2006b, apj, 652, 1531

Migdal A. B., 1959, nphysa, 13, 655

Mochizuki Y., Izuyama T., 1995, apj, 440, 263

Mochizuki Y., Izuyama T., Tanihata I., 1999, apj, 521, 281

Oppenheimer J. R., Volkoff G. M., 1939, Physical Review, 55, 374

Page D., Prakash M., Lattimer J. M., Steiner A. W., 2011, Physical Review Letters, 106, 081101

Pethick C. J., Ravenhall D. G., 1995, Annual Review of Nuclear and Particle Science, 45, 429

Piekarewicz J., Fattoyev F. J., Horowitz C. J., 2014, prc, 90, 015803

Pines D., Alpar M. A., 1985, nat, 316, 27

Pizzochero P. M., 2011, apjl, 743, L20

Radhakrishnan V., Manchester R. N., 1969, nat, 222, 228

Ravenhall D. G., Bennett C. D., Pethick C. J., 1972, Physical Review Letters, 28, 978

Ravenhall D. G., Pethick C. J., Wilson J. R., 1983, Physical Review Letters, 50, 2066

Reichley P. E., Downs G. S., 1969, nat, 222, 229

Roy J., Gupta Y., Lewandowski W., 2012, mnras, 424, 2213

Ruderman M., 1969, nature, 223, 597

Ruderman M., 1976, apj, 203, 213

Ruderman M., 1991a, apj, 366, 261

Ruderman M., 1991b, apj, 382, 587

Ruderman M. A., Sutherland P. G., 1975, apj, 196, 51

Ruderman R., 1991c, apj, 382, 576

Seveso S., Pizzochero P. M., Grill F., Haskell B., 2014, ArXiv e-prints

Shemar S. L., Lyne A. G., 1996, mnras, 282, 677

Shternin P. S., Yakovlev D. G., Heinke C. O., Ho W. C. G., Patnaude D. J., 2011, mnras, 412, L108

Sidery T., Alpar M. A., 2009, mnras, 400, 1859

Smoluchowski R., 1970, Physical Review Letters, 24, 923

Staelin D. H., Reifenstein, III E. C., 1968, Science, 162, 1481

Tong H., 2014, apj, 784, 86

Ushomirsky G., Cutler C., Bildsten L., 2000, mnras, 319, 902

Vivekanand M., 2016, aap, 586, A53

Warszawski L., Melatos A., 2011, mnras, 415, 1611

Warszawski L., Melatos A., Berloff N. G., 2012, prb, 85, 104503

Weltevrede P., Johnston S., Espinoza C. M., 2011, mnras, 411, 1917

Wong T., Backer D. C., Lyne A. G., 2001, apj, 548, 447

Wright G., 2005, The Observatory, 125, 338

Yu M. et al., 2013, mnras, 429, 688